1962

Axial turbulent flow in a circular pipe containing a fixed eccentric core

Robert A. Wolffe
Lehigh University

AXIAL TURBULENT FLOW IN A CIRCULAR PIPE CONTAINING A FIXED ECCENTRIC CORE

by

Robert A. Wolffe

A Research Report
Presented to the Graduate Faculty
of Lehigh University
in Candidacy for the Degree of
MASTER OF SCIENCE

Lehigh University
Bethlehem, Pennsylvania
1962

CERTIFICATE OF APPROVAL

This research report is accepted and approved in partial fulfillment of the requirements for the degree of Master of Science in Chemical Engineering.

(Date)

(Professor in Charge)

(Head of the Department)

ACKNOWLEDGEMENT

The author wishes to thank Dr. Curtis W. Clump for his direction and critical analysis of this work, and Donald G. Young for his immeasurable assistance in all phases of the research.

Further acknowledgement is due to Fred Cataneo for he constructed the major components of the experimental system for his doctoral research, and to Barry Tiernan for donating his time freely to help the author in the early stages of the experimental work.

Finally thanks are due to Joseph Hojsak for his assistance in the fabrication of component parts of the system, and to John Glomb and other fellow graduate students for their helpful suggestions offered during the course of the research.

TABLE OF CONTENTS

LIST OF FIGURES

ABSTRACT

The turbulent flow of air through a circular pipe containing a fixed eccentric core was investigated at one air flow and one fixed eccentricity. The center core was a 2.000 inch I.D. aluminum pipe positioned with its center one quarter of an inch from the center of a 3.082inch I.D. aluminum pipe. Point velocities were measured in the annular space employing an impact tube, fashioned from .042 inch O.D. hypodermic tubing, and a 1/16 inch diameter static wall tap. Axial pressure drop was also measured using two static taps spaced exactly one axial foot apart. All pressure differentials between the impact pressure and the static wall pressure were measured using a highly sensitive micromanometer.

Sufficient velocity data was taken so that a complete velocity pattern for the system could be calculated. Lines of constant velocity and the locus of maximum velocity were determined for the steady turbulent flow in the eccentric system.

By employing the method of Deissler and Taylor and using the universal velocity distribution u^+ , y^+ relationships point velocities were calculated from the measured axial pressure drop. The point velocities calculated in this manner in most cases agreed well with those experimentally determined. The method of Deissler and Taylor also indicated that the

location of the maximum velocity line was accurate for it satisfied the pressure and shear balances used in the velocity calculations.

Both the rigorous solution of the Navier Stokes equation given by Heyda, and the Noyes approximate solution for the location of the points of maximum velocity, are presented and compared with the experimental data. The measured maximum velocity locus for turbulent flow agreed well with that calculated by the rigorous and approximate methods.

From the results of this work suggestions are made for further investigations in this area.

INTRODUCTION

In recent years interest has been expressed in the turbulent flow phenomena existing in non-circular flow systems. In 1955 Deissler and Taylor of NASA published "Analysis of Fully Developed Turbulent Heat Transfer and Flow in an Annulus with Various Eccentricities" (3). In the section dealing with the analysis of turbulent flow Deissler and Taylor combined a simple force balance and the universal velocity distribution equation and developed an iterative geometric method for the solution of the lines of constant velocity and for the maximum velocity locus in an eccentric system. In their method it is necessary to approximate both the maxima locus and the velocity gradient lines to start each trial. Failure in a trial solution calls for adjustment of these assumed lines. As a result of the iterative geometric solution Deisslers method is rather awkward to handle. Heyda (5) devised a method for the calculation of the point velocities in turbulent flow using a trial and error method but not requiring the geometric construction of Deissler's method. Heyda's main assumption is that the location of the maxima locus is the same for the turbulent and laminar case. This assumption had been made for other annular systems before by Rothfus (12) and others (7,11,14). With this assumption Heyda then proceeded to solve the Navier Stokes equation in bipolar coordinates for the laminar flow case. An outline of this development is

presented in Appendix B-1. Heyda obtained a rigorous equation defining the location of the maxima locus for laminar flow. Solution of this equation is somewhat difficult and Noyes suggested a simple equation affording an approximate solution for the locus of maxima. Heyda presents analytical data showing the accuracy of the Noyes approximation to be fair but to create some definite error. Employing the calculated maxima locus and using Van Driest's universal velocity distribution relations Heyda developed an iterative procedure for defining point velocities.

The purpose of the work reported here was to make accurate velocity measurements throughout an annular eccentric space and to calculate the resulting iso-velocity lines and the locus of maxima. The major equipment employed in this investigation was that used in a previous study of mass and momentum transfer from a napthalene core positioned concentrically inside of a 3 inch pipe. The equipment was modified for eccentric core alignment and a method of sampling the total area of the annular space of the flowing stream was developed.

DESCRIPTION OF APPARATUS

General: Refer to Figure 1

A. Air Supply from a moderately high capacity blower (260 cfm against 2 p.s.i.) was brought to temperature via banks of finned heaters, contained in surge tank downstream of the blower. The air mass flow rate was controlled by the bleed valve V1, at the blower outlet, and V2. A portion of the heated air was passed through the inner core in order to minimize thermal gradients in the system.

B. The Annulus was composed of an 11 foot upstream calming section, corresponding to 132 equivalent diameters, a 5 foot test section and an 8 foot downstream calming section thus ensuring nearly fully developed, undisturbed turbulent flow at the test section.

C. The Sampling Apparatus was arranged to obtain point impact pressures for the determination of the velocity distribution in the annulus. A standard impact tube fabricated from hypodermic tubing (0.042 inch O.D., .0075 inch wall) was used for this purpose. A micrometer feed mechanism, similar to that described by Rothfus (10), was mounted on the shell tube of the annulus so that by rotation of the outer shell the impact tube could be reproducibly positioned at any point in the annulus to .001 of an inch. Pressure readings were taken from a precise micromanometer accurate to .001 inch water for velocity pressures

FIGURE 1

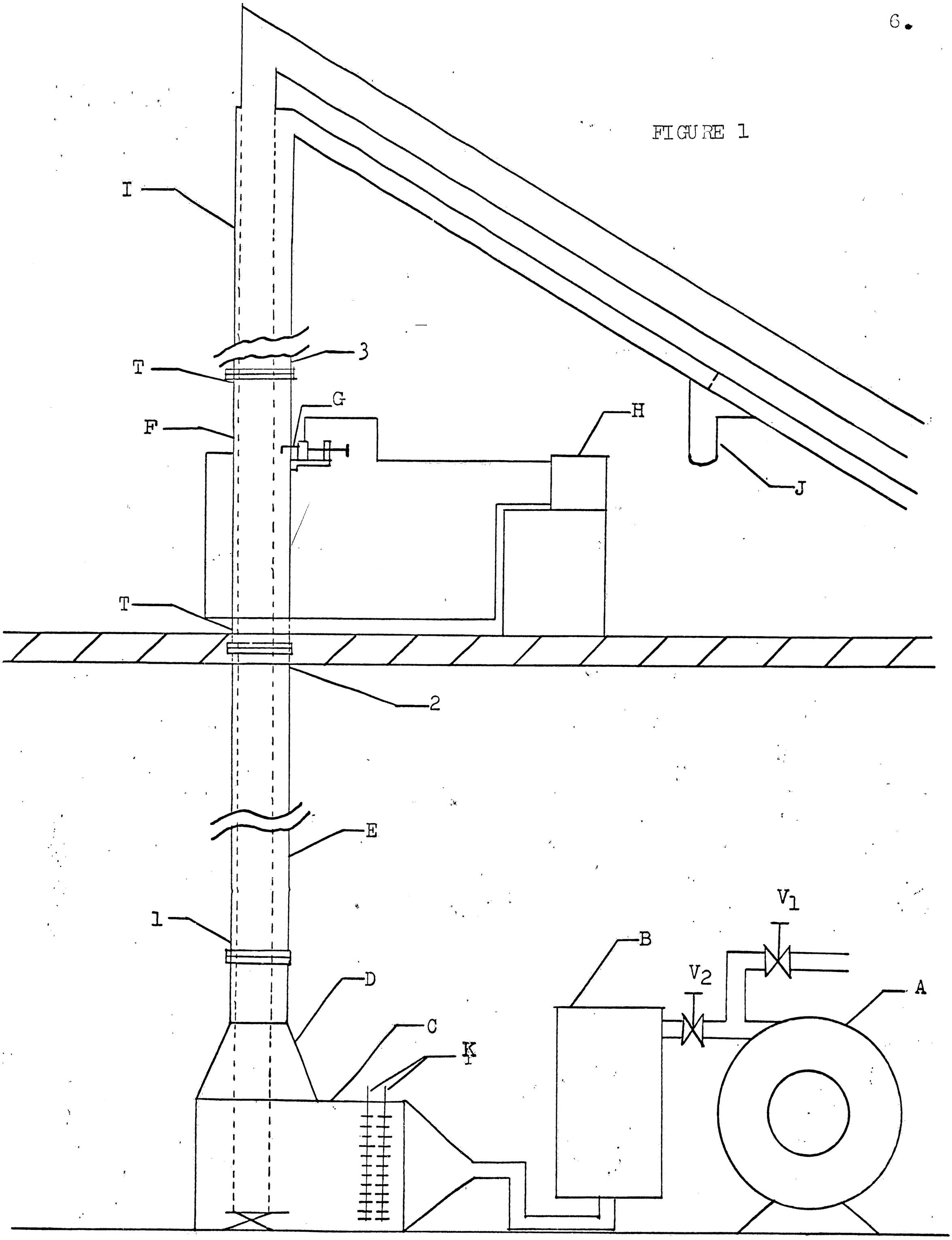

DIAGRAM OF APPARATUS

FIGURE 1

NOTATION

A. Blower

B. Entrainment remover

C. Surge Tank

D. Converging section

E. Upstream calming section

F. Test Section

G. Impact tube with micrometer feed mechanism

H. Micromanometer

I. Downstream calming section

J. Orifice meter

K. Finned heaters

T. Thermocouple locations

V1. Globe valve

V2. Globe valve

1,2,3. Locations of core positioning screws

less than .2 inch water.

The Blower - The blower was a sliding vane type ("High Pressure Blower No. 4" built by the American Gas Furnace Company, Elizabeth, N.J.) capable of moving 260 ft^3 air/minute against a pressure of 2 psi. The blower was disassembled, cleaned, and had new Babbitt bearings installed before it was reassembled and placed back in the system. Since the discharge from the compressors is inherently pulsating, and pulsation would be an added variable of unknown magnitude in the flowing system, surge volumes were incorporated into the system upstream of the annulus.

The Surge Tank - The galvanized sheet steel surge tank performed several functions not indicated by its title. It acted to support the annular core, which rested on a jack contained therein, and to give partial support to the shell, which was anchored by standard wall pipe supports. In addition, it housed two banks of finned heaters, one heated by steam and the other electrically heated. The steam bank was composed of three independent finned tubes, each having a finned length of 22 inches. The electrical resistance bank, composed of "Chromolox" SEF series heaters, had two 500 watt, and three 250 watt heaters, each being independently controlled. One of the heaters was connected to a variable transformer to allow fine temperature regulation.

The title function of the surge tank was aided by the presence of a converging conical section, having a 12 inch base, which like the annulus was fabricated of aluminum. A 6 inch

length of 3.5 inch aluminum pipe was arc welded to the top of the section to faciliate connection to the annular shell. The base was attached to the sheet steel tank by a gasketed flange connection. A section of 28 mesh stainless steel gauze placed across the path, and held rigidly along with the flanged gasket, reduced still further the turbulent fluctuations produced by the blower. The design and location of the gauze and of the converging section were in accordance with Pankhurst (8).

In order to remove possible swirls in the air flow developed in the converging section, four symetrically placed straightening vanes (fashioned from sheet aluminum) were installed immediately downstream of the test section. These vanes, which also served to position the core of the annulus, were rectangular, 12 inches long and 0.8 inch, 0.5 inch, and 0.27 inch in width. They were held rigidly in milled slots provided on the annular core via force fit and epoxy resin.

Additional surge volume was provided by the entrainment remover immediately upstream of the surge tank. The unit, constructed from a 50 gallon drum, contained fiber glass filters to trap any oil entrained in the airflow from the blower.

The Annulus

The shell: 3 inch standard extruded aluminum pipe.

The Core: 2 inch O.D., 0.125 inch wall, round aluminum tube.

The core as well as the shell, consisted of three sections 11 feet,

5 feet, and 8 feet in length. The test section shell, the 5 foot section, was connected to two 6 inch shell sections which were in turn connected to the upstream and downstream sections. Since the shell part of the test section had to be free to rotate, and thus enable impact traverses at all points, it was necessary to modify the jointure method from that previously used in the mass transfer study. To hold the shell tube in perfect alignment during all turning operations an upper double sleeve support was constructed. This consisted of one stationary clamp which held firmly the downstream connecting collar, and a second clamp stabily connected to the downstream clamp holding the downstream end of the test section shell. The test section clamp was lined with a soft felt material which enabled the shell to be turned while being held relatively firmly by the clamp. A picture of this downstream mating alignment device is shown in Figure 2.

To assure a constant eccentric alignment of the inner core with respect to the shell three sets of specially constructed setscrews located 120° apart on the shell periphery were used at three longitudinal positions. These setscrews were designed so that only a 1/16 inch diameter rod protruded into the flow field, the screw portion remaining entirely in the shell wall. The measurement of core to wall distances was preformed employing the normal impact tube feed mechanism and a vacuum tube test meter. The impact tube was insulated from the outer shell wall by a teflon plug and electrical tape. The common lead from the meter was

SYSTEM ALIGNMENT

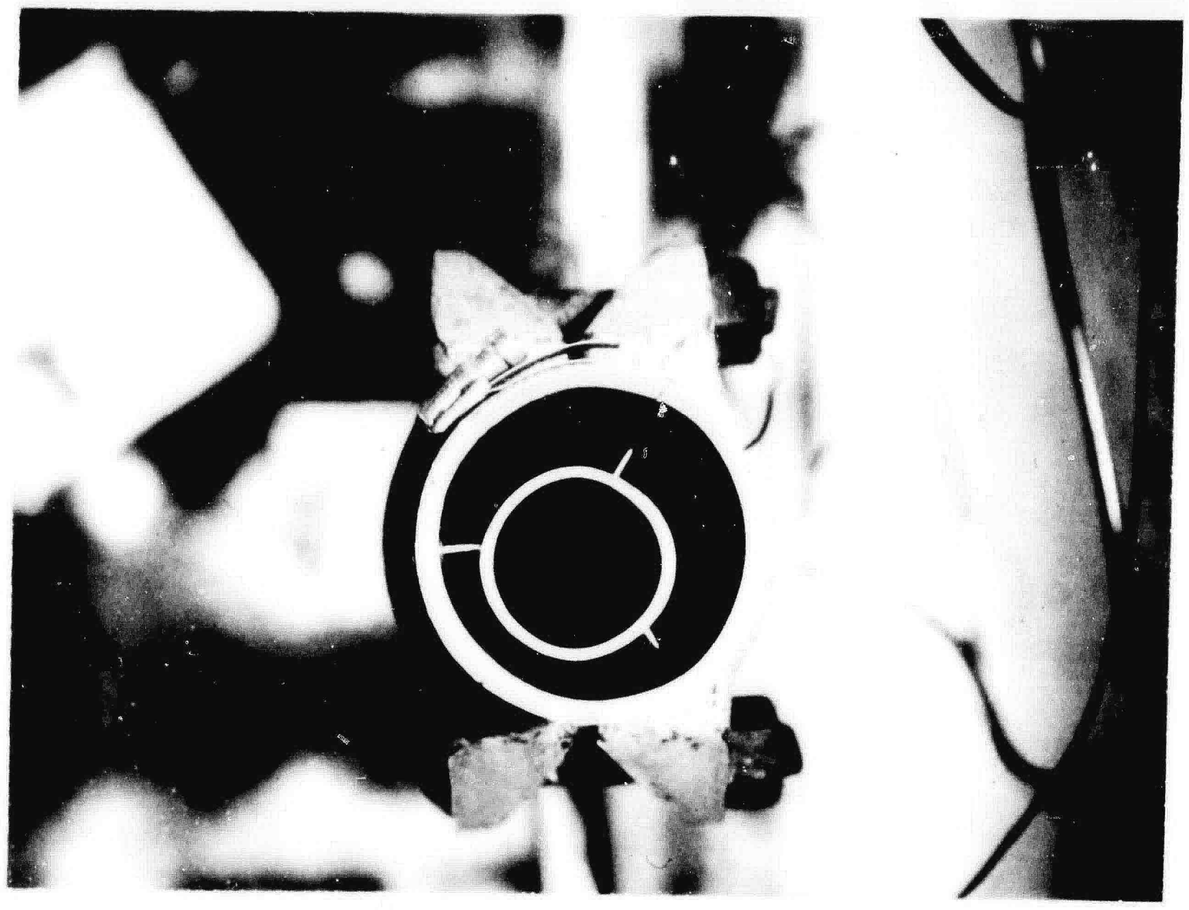

CORE ALIGNMENT

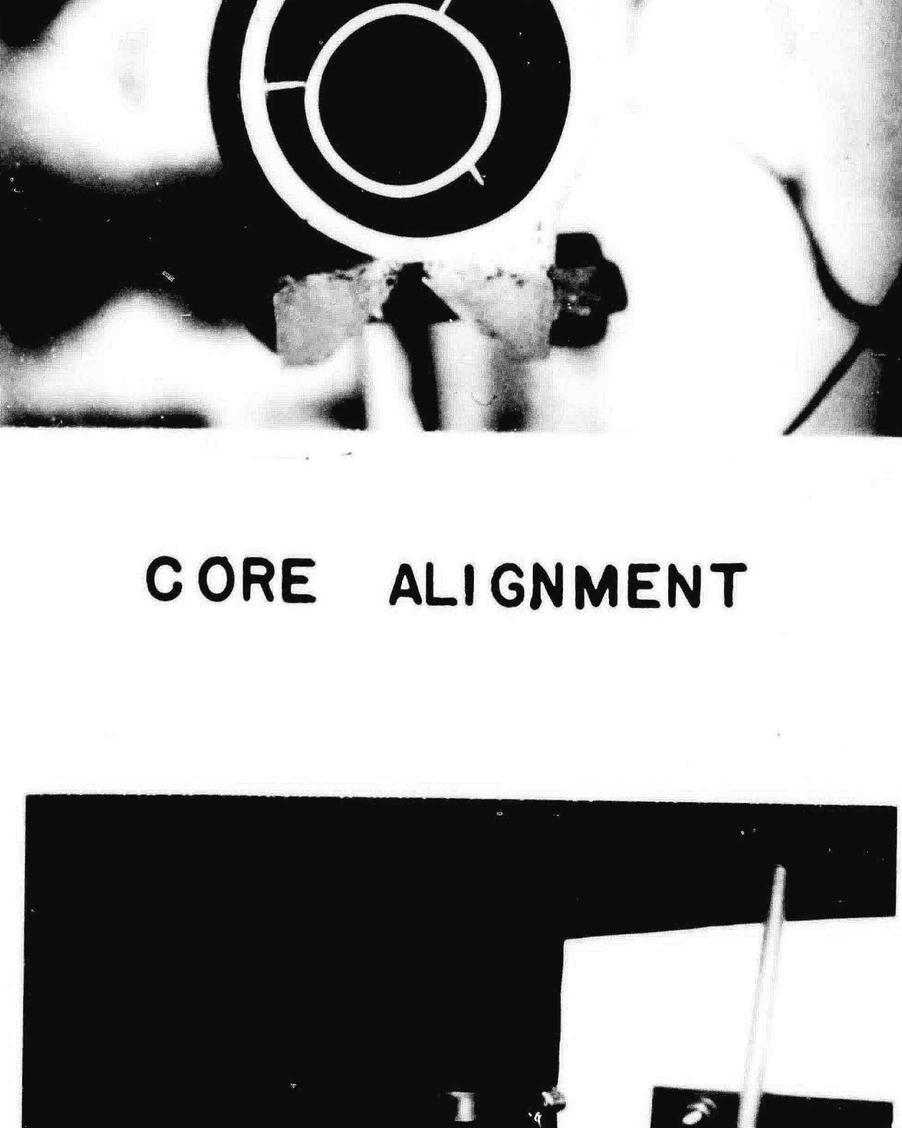

SHELL ALIGNMENT

FIGURE 2

attached to the impact tube and the ohm lead to the annulus. When the impact tube touched either the outer shell or the inner core the meter showed a large change in resistance and thus contact was known. Measurements were taken on the impact feed mechanism as explained later. This method of measurement gave values of traverse distances reproducible to .001 inch. The impact tube packing gland is similar to one used by Rothfus (10).

Static pressure taps were made diametrically opposite to the impact tube openings in the annulus. The holes were made according to the rigid specifications stated by Folsom (4). They were accordingly a 1/16 diameter hole drilled perpendicular to the pipe well with all burrs carefully removed with steel wool. A gasketed curved cover plate connection, fashioned from a 3 inch length of 3.5 inch I.D. pipe (which fit snuggly over the 3.5 inch O.D. test section pipe) cut along its longitudinal axis was used. The necessary compression fitting was attached only to the cover plate, which was subsequently used to sandwich a piece of 1/16 inch soft sheet rubber, equipped with a 1/8 inch D hole, against the test section. The assembly was then held together with worm gear type hose clamps.

To maintain temperature control the entire annular shell was wrapped with standard glass fiber heating taps in circuit with a Fenwall thermo-switch set at 105 F. The entire assembly was then covered with standard split corrugated pipe insulation. Themocouples placed at two points along the test section provided

accurate indication of temperature. System thermocouples were arranged to lead to a rotary switch which was connected to a Leeds & Northrup potentiometer. Each thermocouple was calibrated relative to an accurately calibrated thermometer (accurate to .10) employing water at different temperatures contained in a well insulated Dewar Flask. See Appendix D.

The Sampling Apparatus - The impact tube was positioned in the annulus to .001 inch by a micrometer feed mechanism similar to that previously described by Rothfus (*10*). The feed mechanism was supported directly on the outer shell and held firmly so that all space in the annulus could be traversed by turning the shell part of the test section while holding the rest of the system rigid. The magnitude of the coefficient Ci of the impact tube equation $u = Ci\sqrt{2g_c \frac{\Delta P}{\rho}}$ was taken as unity according to Folsom (*4*). See Figure *4*.

The Micromanometer - This instrument, shown in Figure *3*, was a null reading hydrostatic device with an accuracy of .001 inch water. Its design was similar in principle to the general description given in (1) of Prandtl's instrument.

The device was essentially a U tube manometer with one moveable leg. The reservoir (A) was attached via a screw connection to a cantilever beam brazed to a collar which could slide vertically on a steel shaft (B). Connected to the reservoir was a piece of plastic tubing (C), providing the linkage to the inclined glass tubing (D) which was part of the rigid leg of the

MICROMANOMETER

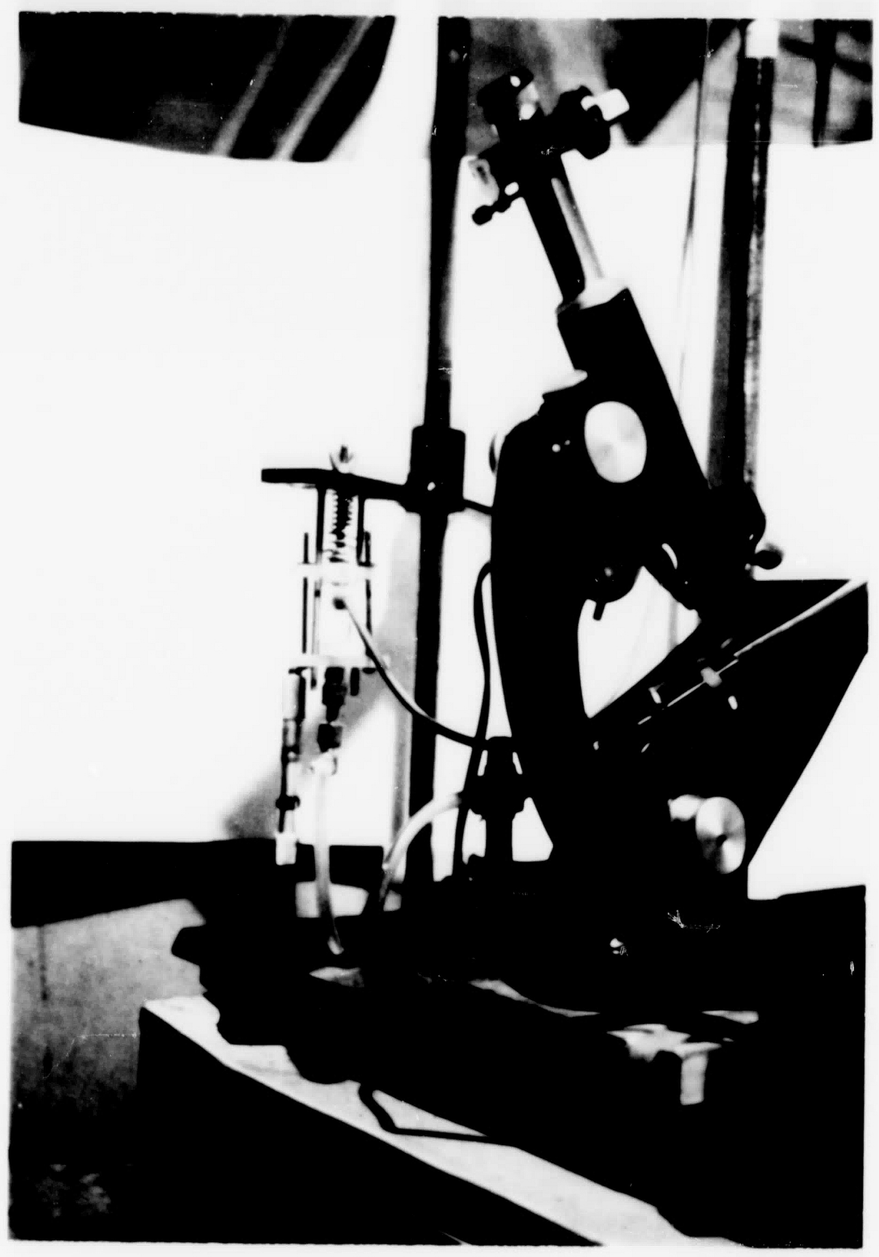

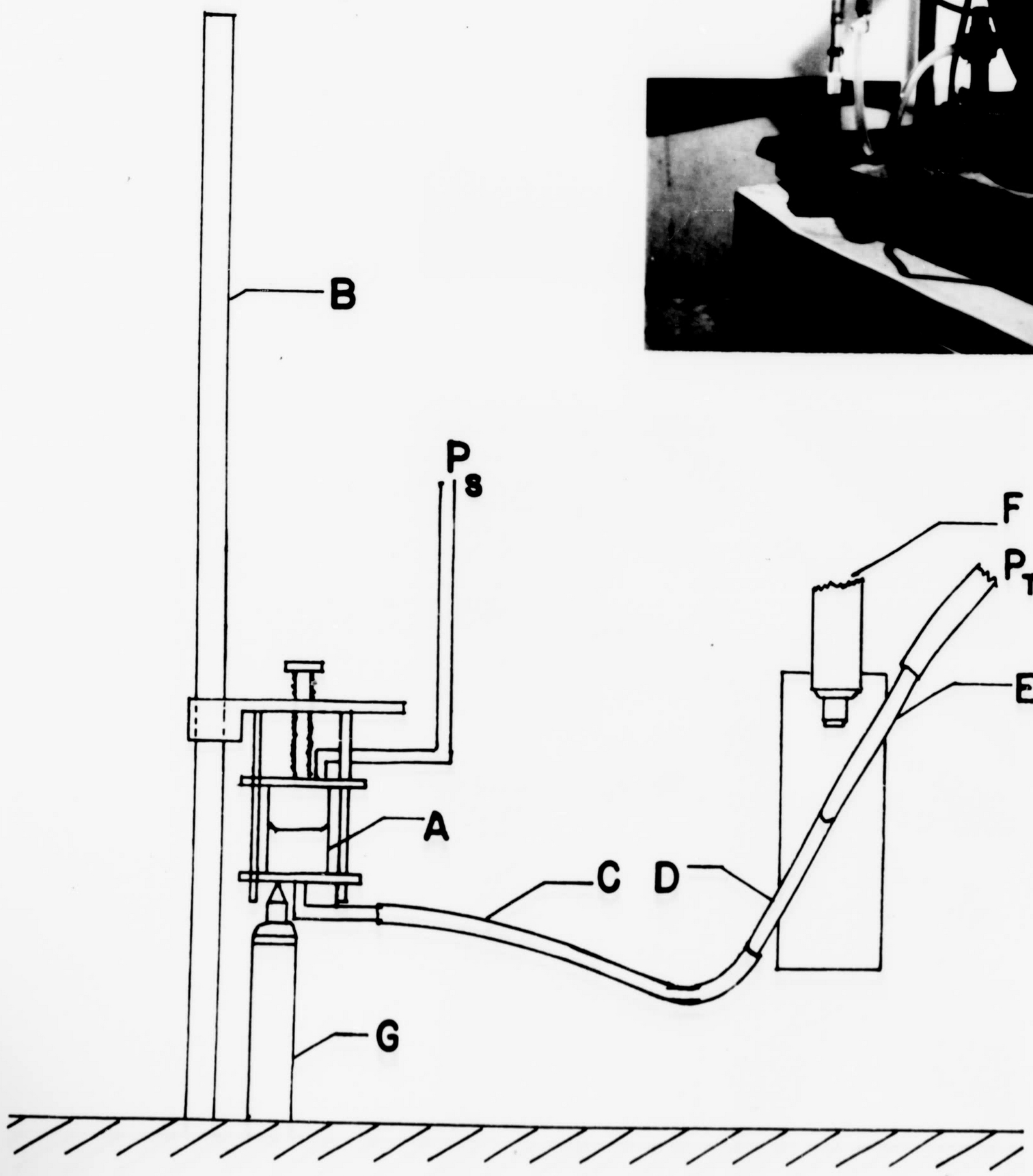

FIGURE 3

IMPACT TUBE & MICROMETER FEED MECHANISM

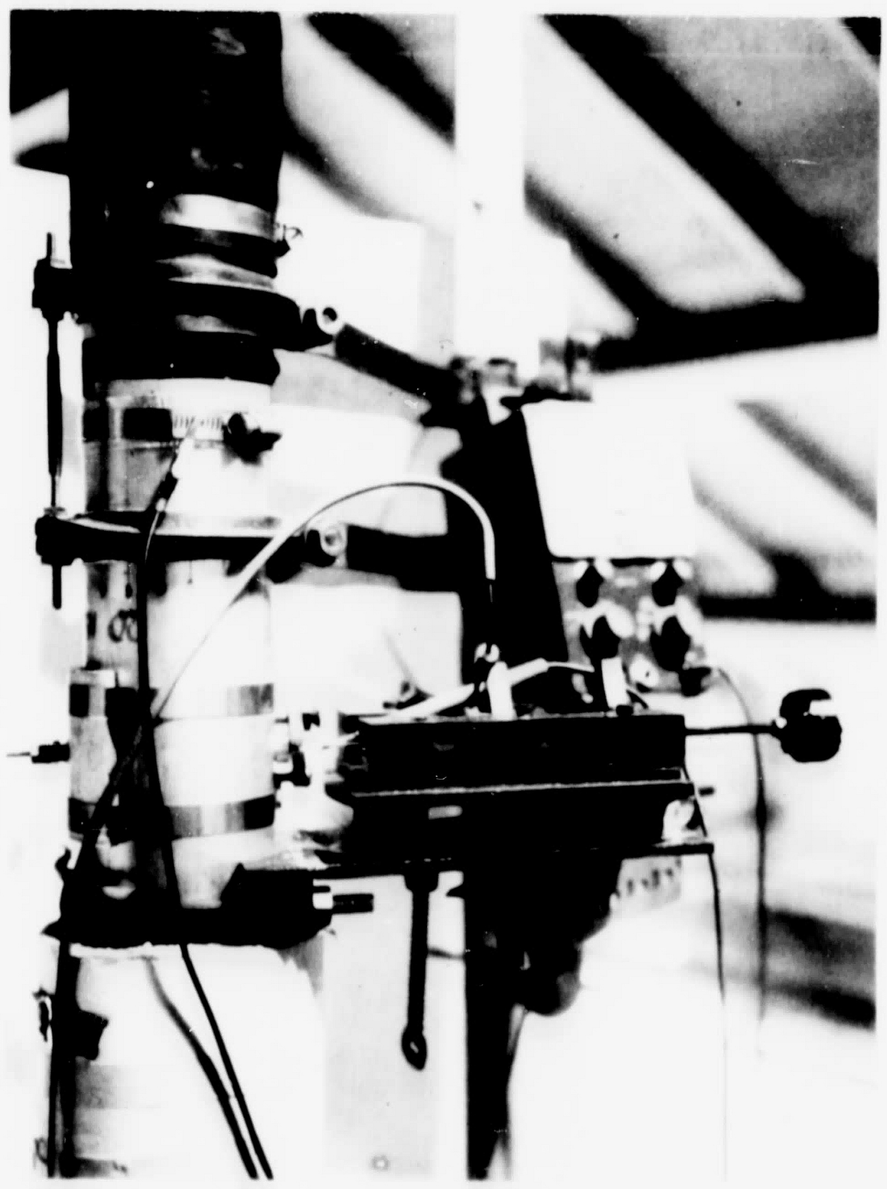

FIGURE 4

U tube (E). The inclined glass capillary tube contained the meniscus of the manometer fluid (G.E. SF-81(50) Silicone oil) whose position was determined with the aid of the microscope (F) to .001 inch of vertical height measured by the inside micrometer.

EXPERIMENTAL PROCEDURE

The preliminary procedure involved the accurate alignment of the eccentric geometry. This necessitated the movement of the center core by means of the positioning screws immediately above and below the test section. The system was modified so that the outer shell with the impact tube feed mechanism mount could be turned without changing traverse distance between the outer wall and the core. Before velocity data was taken it was shown that core shell positioning before and after shell turning could be reproduced to .001 inch.

Once the system was aligned and closed the traverse distance was again measured employing the vacuum tube test meter as the wall-finding instrument. The blower was then started along with the appropriate heaters, depending upon the ambient temperature.

While the system was heating the micromanometer was zeroed and the null readings were taken. The nulling procedure involved removing both pressure hoses from their respective column fittings and shunting the manometer. The reservoir was then lowered so that the meniscus was observed on the lower section of the micromanometer tube in the microscrope field. The reservoir height for this position was then measured using the inside micrometer mounted vertically below the reservoir. The reservoir was then further lowered until the meniscus resided at the

upper section of the microscope field and the reservoir height again measured with the inside micrometer. With these two readings the field sensitivity, i.e., the inches of water equivalent to microscope scale reading, was evaluated. Upon reaching the equilibrium temperature (105° F) the micromanometer leads were replaced on the column fittings, making sure that the manometer shunt was open during the process. The manometer shunt was then closed and the reservoir was raised until the meniscus reappeared on the manometer scale in the microscope field. Reservoir height was then read and the impact tube moved to a new position and the system nulled again as before. Thus successive pressure readings were taken until the complete traverse had been made and then the blower and the heaters were shut off. At the end of a traverse the micromanometer was again nulled and the sensitivity re-evaulated. All traverses were made in an identical manner.

After investigating fully the profiles at a level 4 feet from the bottom of the test section the outer shell was changed and replaced with a shell with the feed mechanism located at a level 2 feet from the bottom of the test section. A traverse was made at this level to check the assumption of fully developed flow. This shell was also equipped with two static pressure taps located 1 foot apart in an axial direction. The axial pressure drop was measured from these two taps employing the micromanometer.

EXPERIMENTAL RESULTS

A. Analysis of Error - The main source of error affecting the velocities calculated was the inherent turbulent fluctuation picked up by the sensitive micromanometer system. Figure 5 shows a typical meniscus history as affected by the impact pressure fluctuations. It should be noted from this figure that while the fluctuations are as great as 1.5 scale readings, corresponding to .004 inches of oil, the average value may be easily estimated to 0.3 scale readings which corresponds to slightly less than .001 inches of oil. It is concluded therefore that the impact tube pressure measurements are accurate to within .001 inches of oil and it has been calculated that this error corresponds to an error in calculated velocity of 0.05 ft/sec for velocities around 40 ft/sec and to about 0.10 ft/sec at velocities in the neighborhood of 20 ft/sec. Other sources of error in measurement of impact pressures could be in vertical alignment of the impact tube and in positioning in precise points in the traverse space.

The traverse alignment distance was measured as in the previous work of Cataneo (2) using an outside micrometer and the measuring blocks on the impact tube feed mechanism. The error involved in this measurement is that of consistent use of the micrometer. It was found that the micrometer could be consistently read to .001 inch. The method for finding the traverse distance between shell and core, employing the on-off resistance measured

MENISCUS POSITION VS. TIME

RUN 42

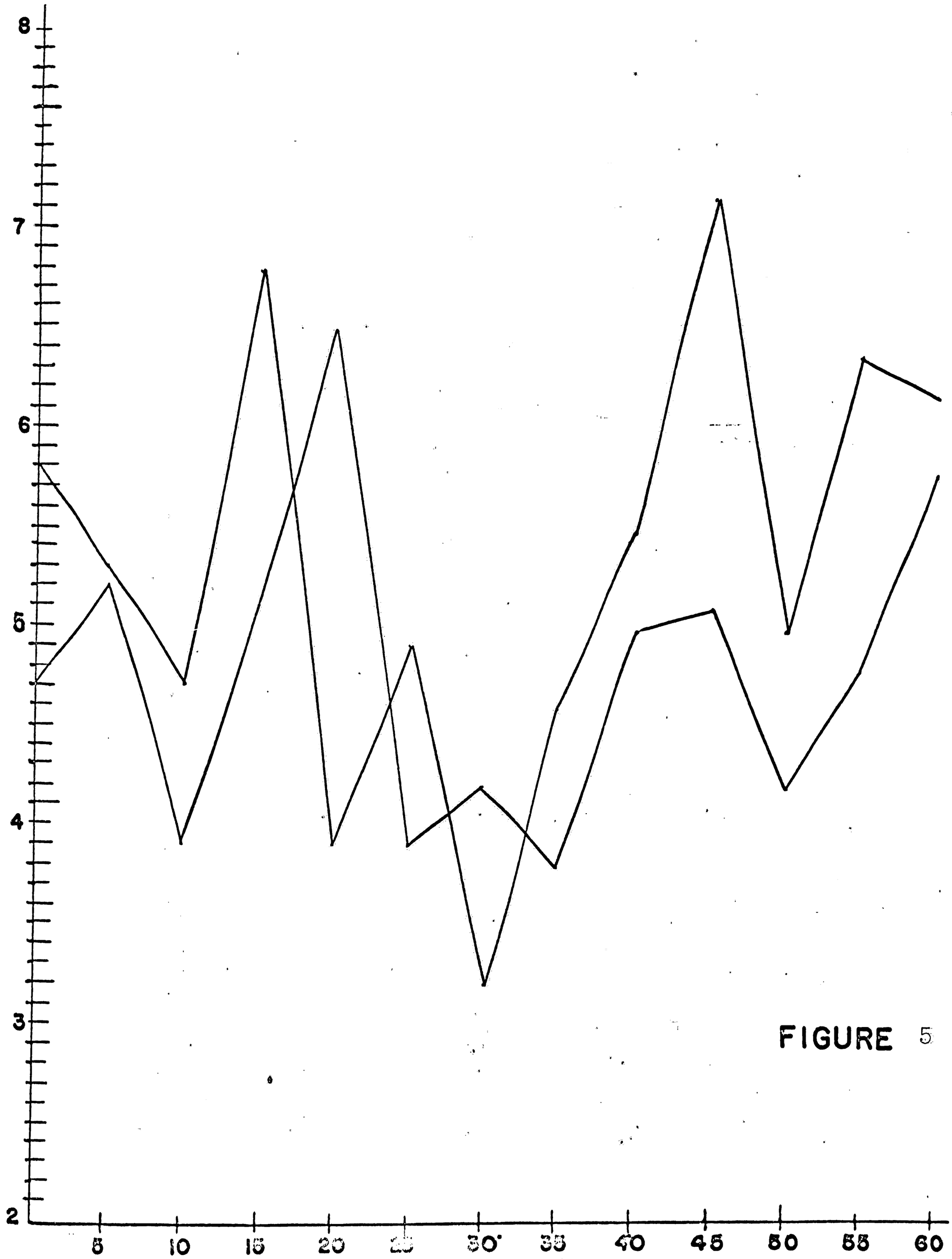

FIGURE 5

by the vacuum tube test meter, gave measurements reproducible to .001 inch, or to the limit of the micrometer used for measurement.

While it was possible to maintain an eccentric position to .001 inch, it was found that the traverse distance did not in all cases correspond to those calculated for a 2.000 in O.D. pipe inside of a 3.082 in I.D. pipe. It was found that traverse distances differed from the calculated by as much as .02 inch. It was concluded that this error produced by the .01 inch tolerance of the extruded aluminum pipe and not by the alignment system. The error associated with these displacements is significant only for the shorter traverse distances at 180° and 200°.

The velocity traverses presented in Figures 6 through 12 present point velocities measured during at least two different runs and in the case of the 40° traverse, Figure 8, three runs at a total of two levels in the test section. In all cases it is seen that the agreement between runs is sufficient to allow the construction of a smooth profile through all the points calculated. The three runs calculated for the 40° traverse verify the assumption of steady flow in the annulus.

In preliminary runs (runs 3 to 13) taken before the alignment procedure was perfected it was observed that the alignment set screws interfered with the flow pattern directly past them for a distance of at least 7 inches. This was evidenced by the fact that the maximum velocity at an axial distance of 7 inches above

the 0° alignment screw, which is the largest annular space, was 3 ft/sec lower than the maximum velocity measured at traverses 40° displaced from the maximum 0° traverse. As a result of this, all test data was taken at a level more than four feet above the alignment screws and thus past the minor perturbation caused by their presence.

B. Comparison of the Velocity Profiles with Profiles Predicted by the Method of Deissler and Taylor - In the Deissler and Taylor method, which is outlined in detail in Appendix A-1, an iterative procedure is followed to locate the locus of maximum velocity in the annulus and to establish the velocity gradient lines. This procedure involves the geometric approximation of the location of these lines and the calculation of a force and stress balance on areas defined by the bounding velocity gradient lines, the physical boundaries, and the line of maximum velocity. In conjunction with this force balance the universal velocity distribution equations of von Karman (/3) are applied and the subsequent velocity profiles for traverses perpendicular to the shell boundary are calculated. The results of these calculations are significant for two reasons. First, the force balances made employing the measured locus of maximum velocity and velocity gradient verified the fact that the measurement of the locus of maxima was correct. Secondly, the velocity profiles calculated using the universal velocity distribution of von Karman showed agreement within 4 percent of the experimentally measured numbers for all

EXPERIMENTALLY DETERMINED VELOCITY PROFILE TURBULENT FLOW IN AN ECCENTRIC ANNULUS

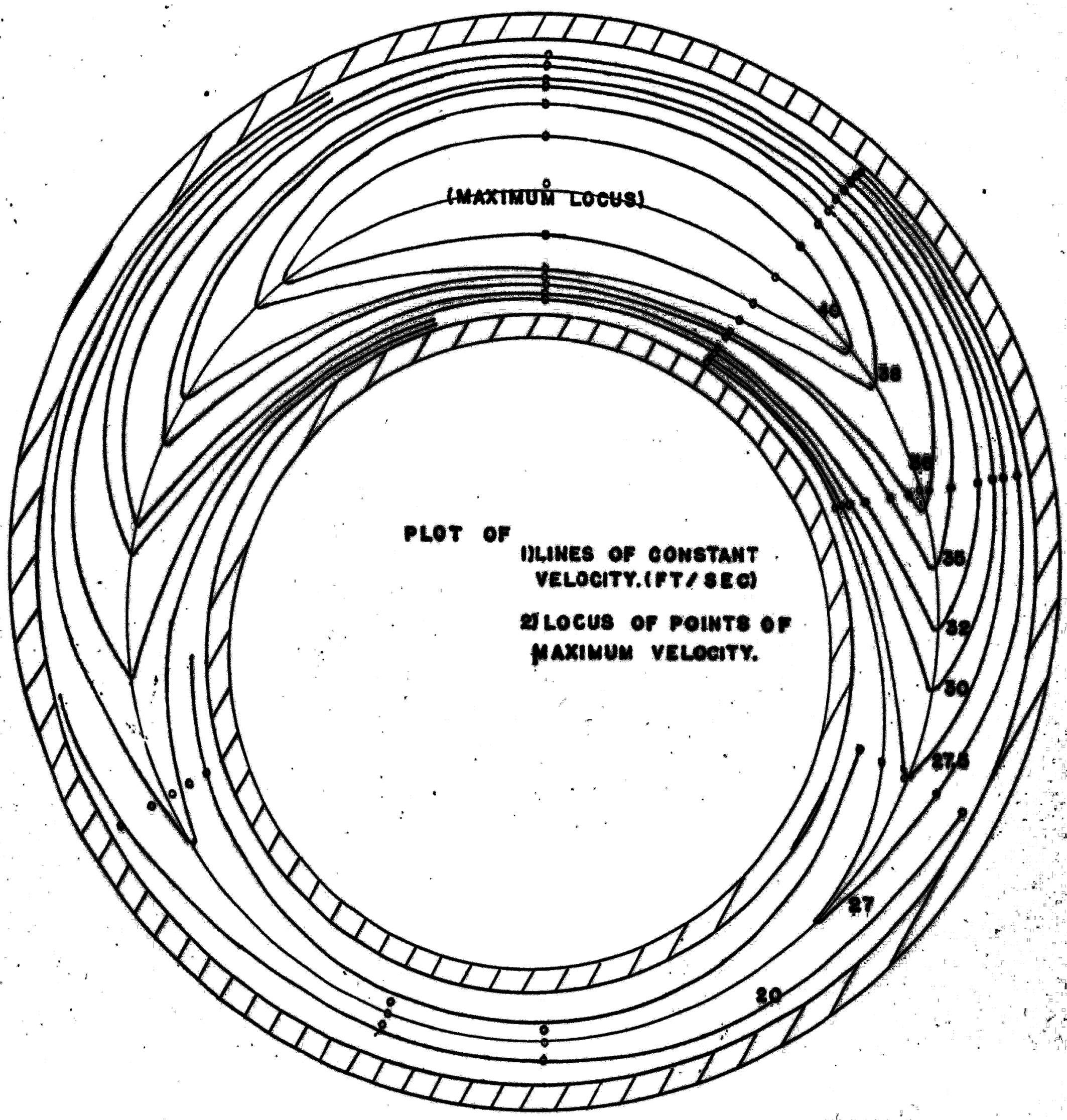

PLOT OF

1) LINES OF CONSTANT VELOCITY. (FT/SEC)

2) LOCUS OF POINTS OF MAXIMUM VELOCITY.

FIGURE 6

VELOCITY PROFILE
0°

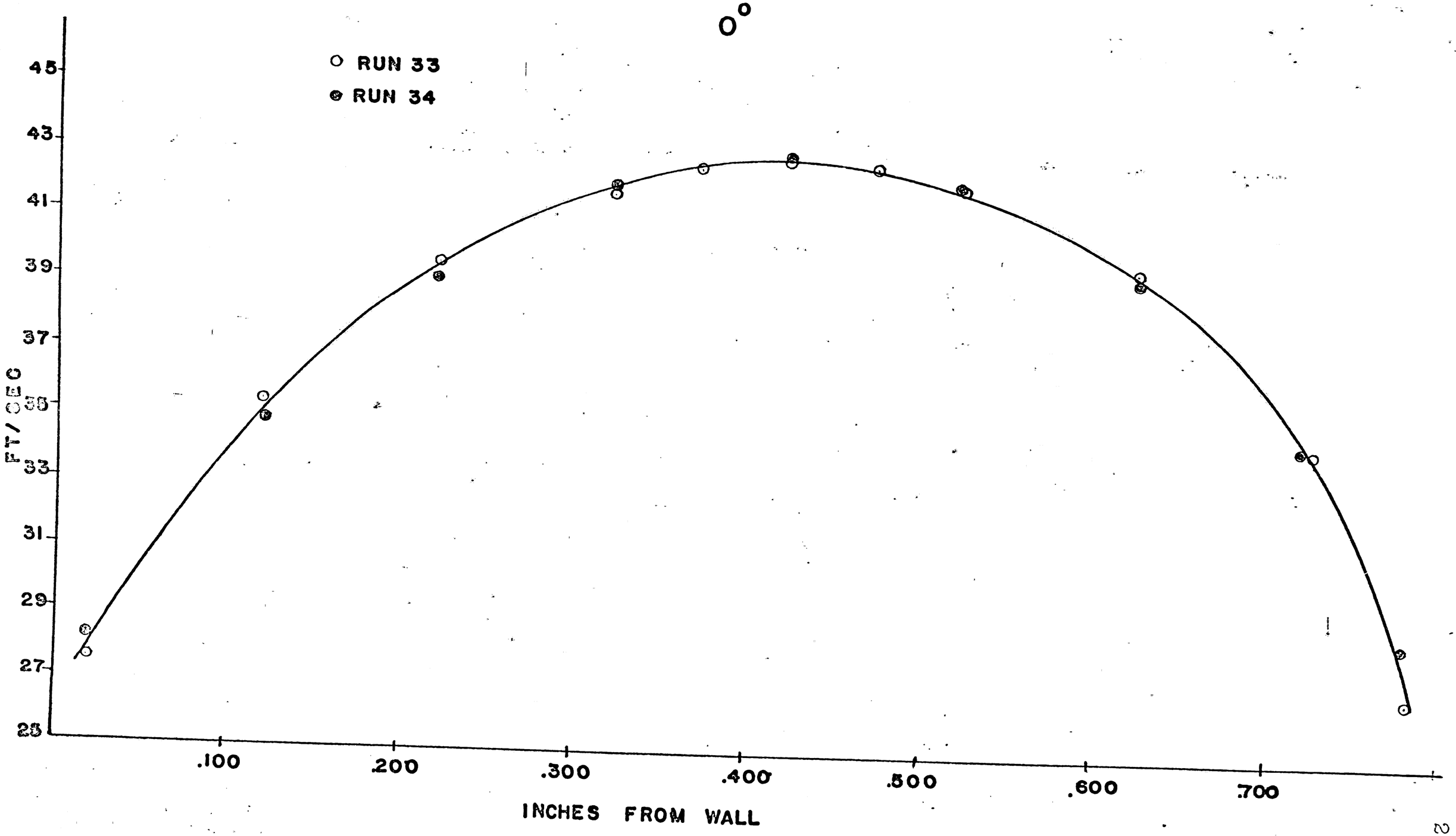

FIGURE 7

VELOCITY PROFILE

40^{0}

▽ RUN 45 (2 FT LEVEL)
○ RUN 41 (4 FT LEVEL)
⊛ RUN 36 (4 FT LEVEL)
X UNIVERSAL VELOCITY DISTRIBUTION

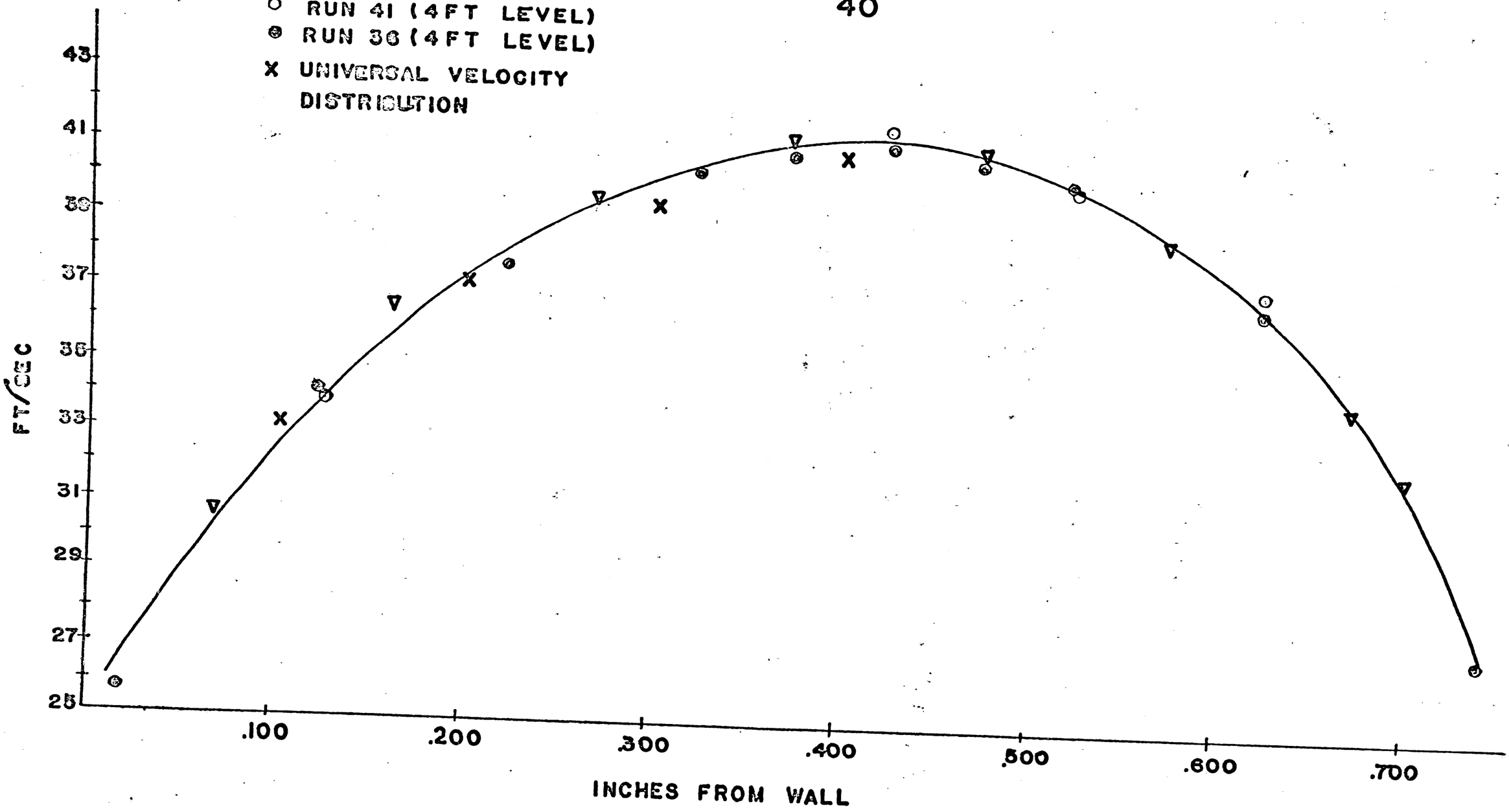

FIGURE 8

VELOCITY PROFILE

80°

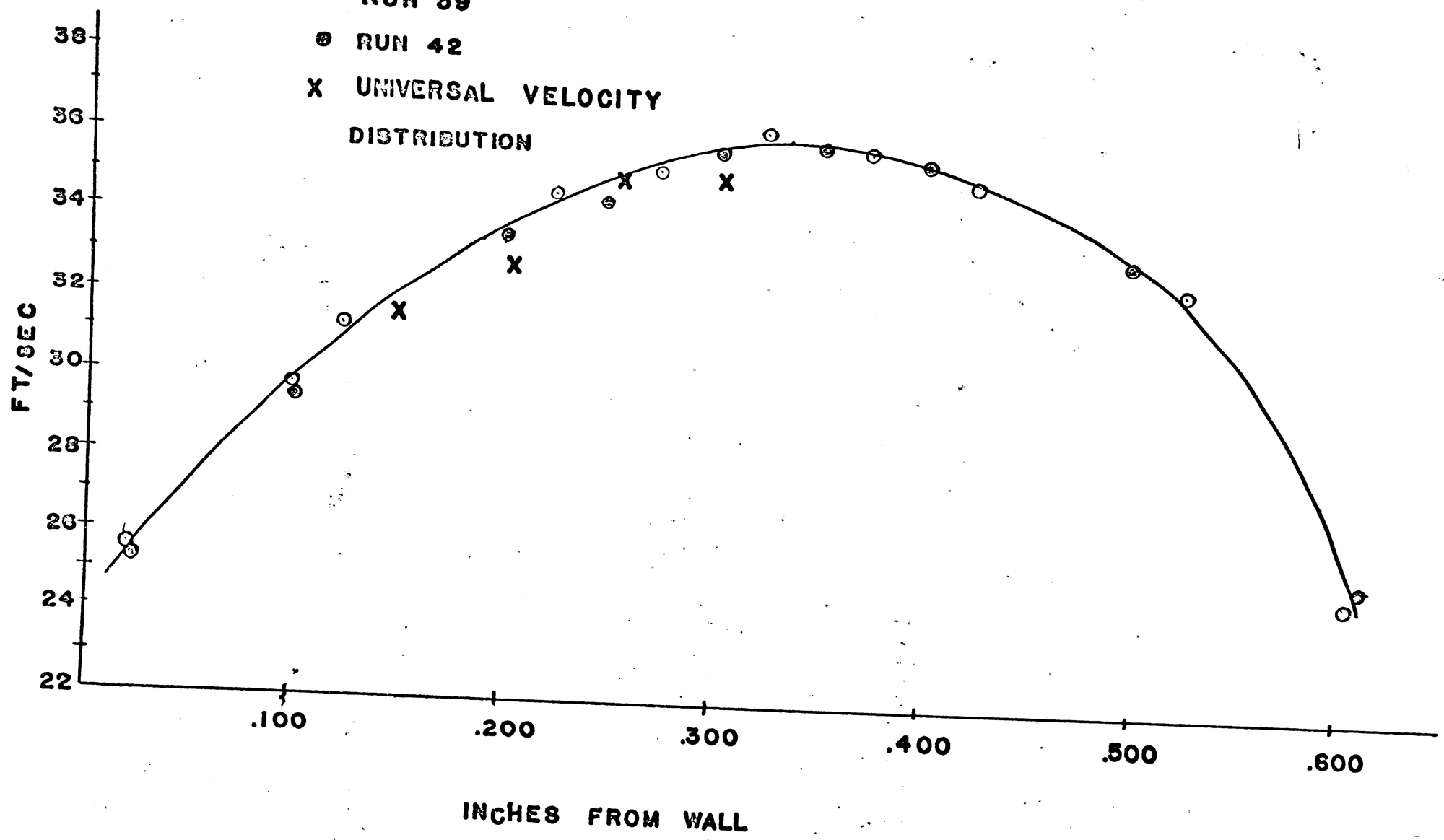

FIGURE 9

VELOCITY PROFILE

120°

RUN 35

X UNIVERSAL VELOCITY DISTRIBUTION

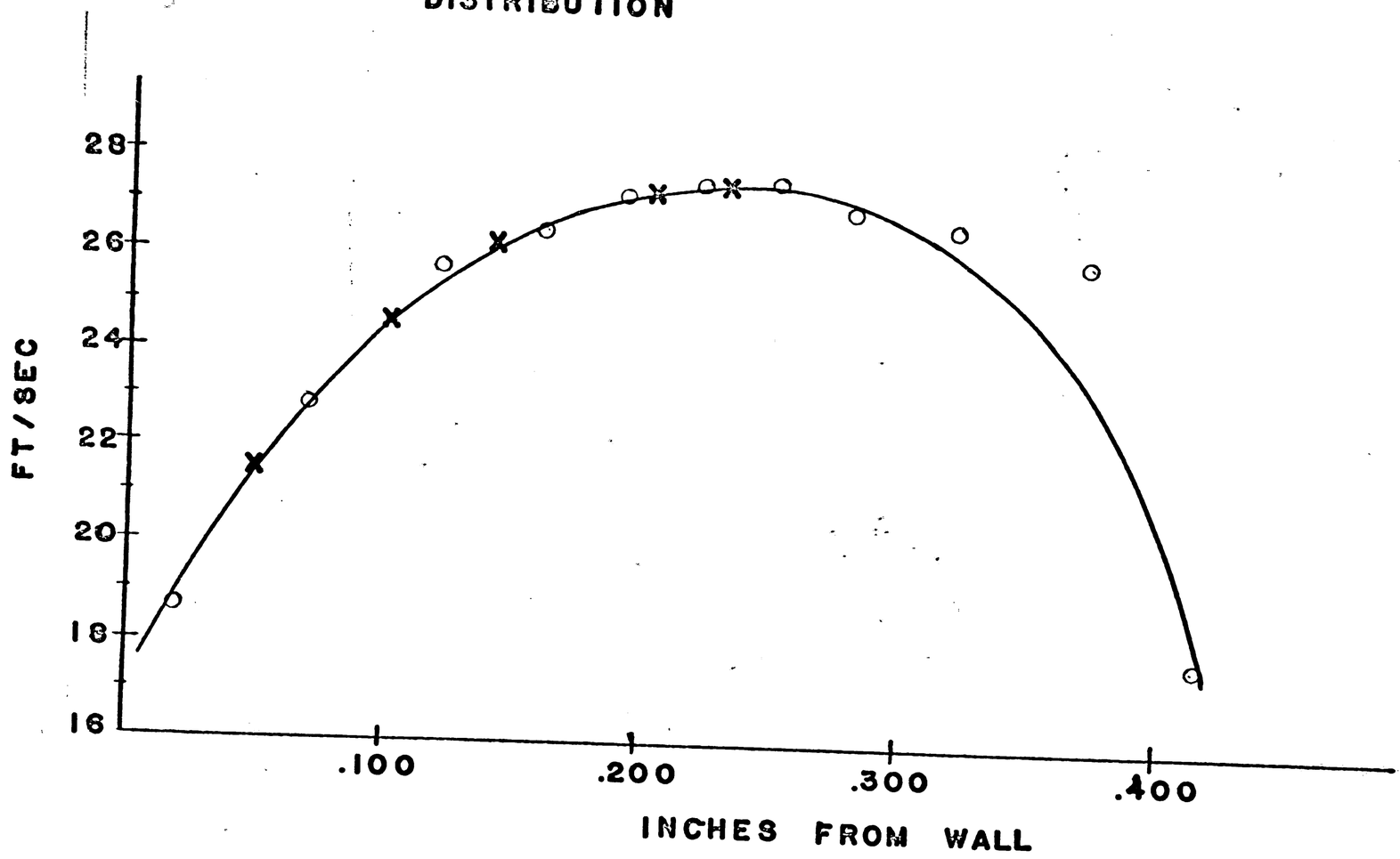

FIGURE 10

VELOCITY PROFILES

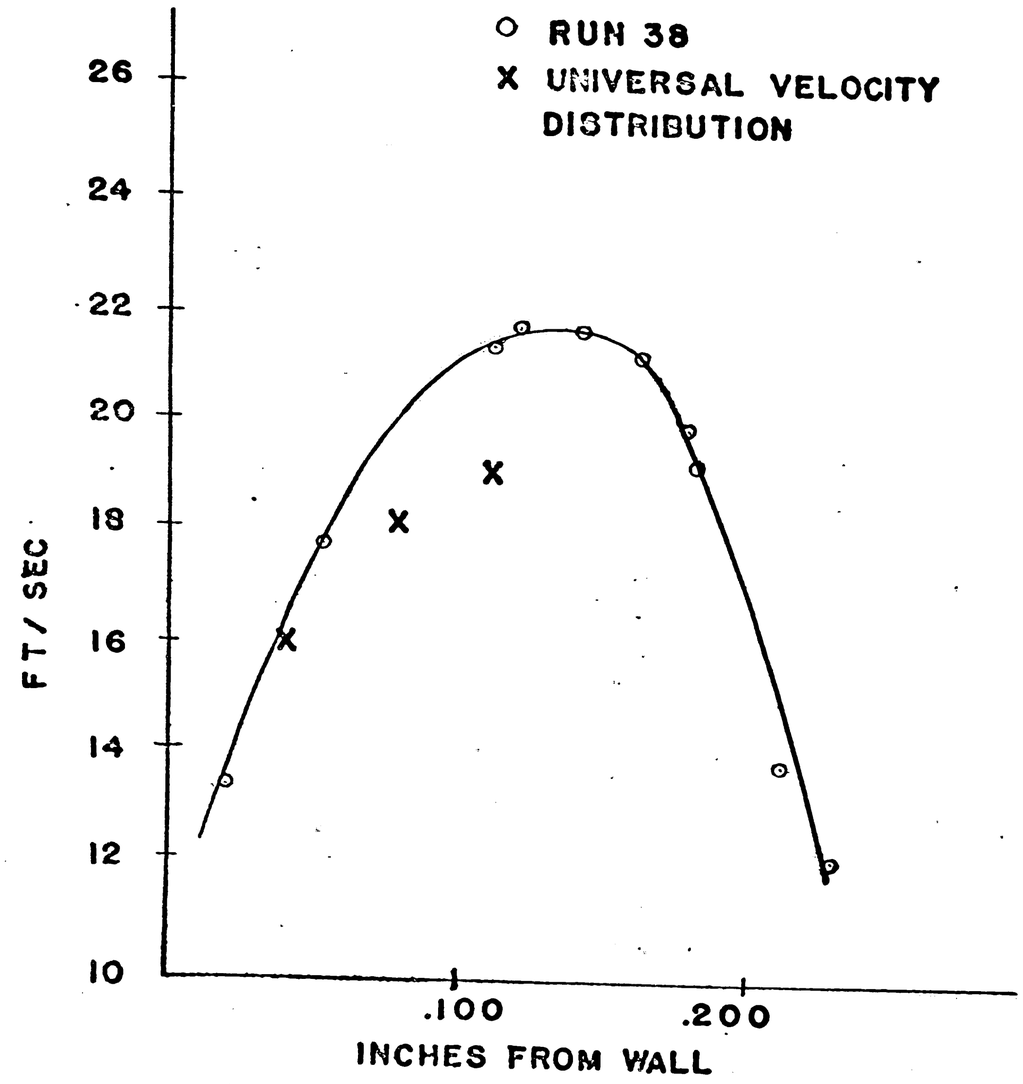

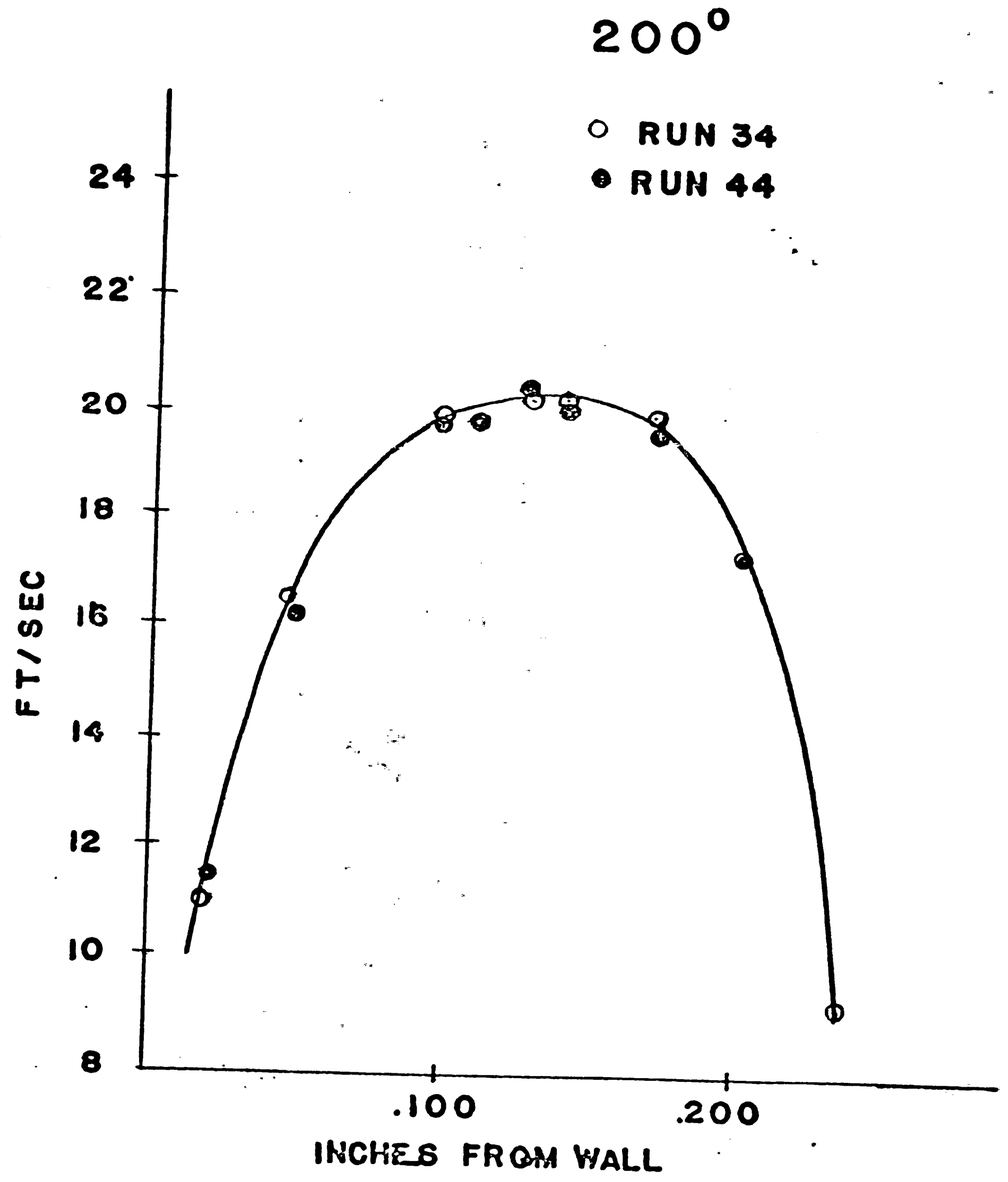

FIGURE 11

VELOCITY PROFILES

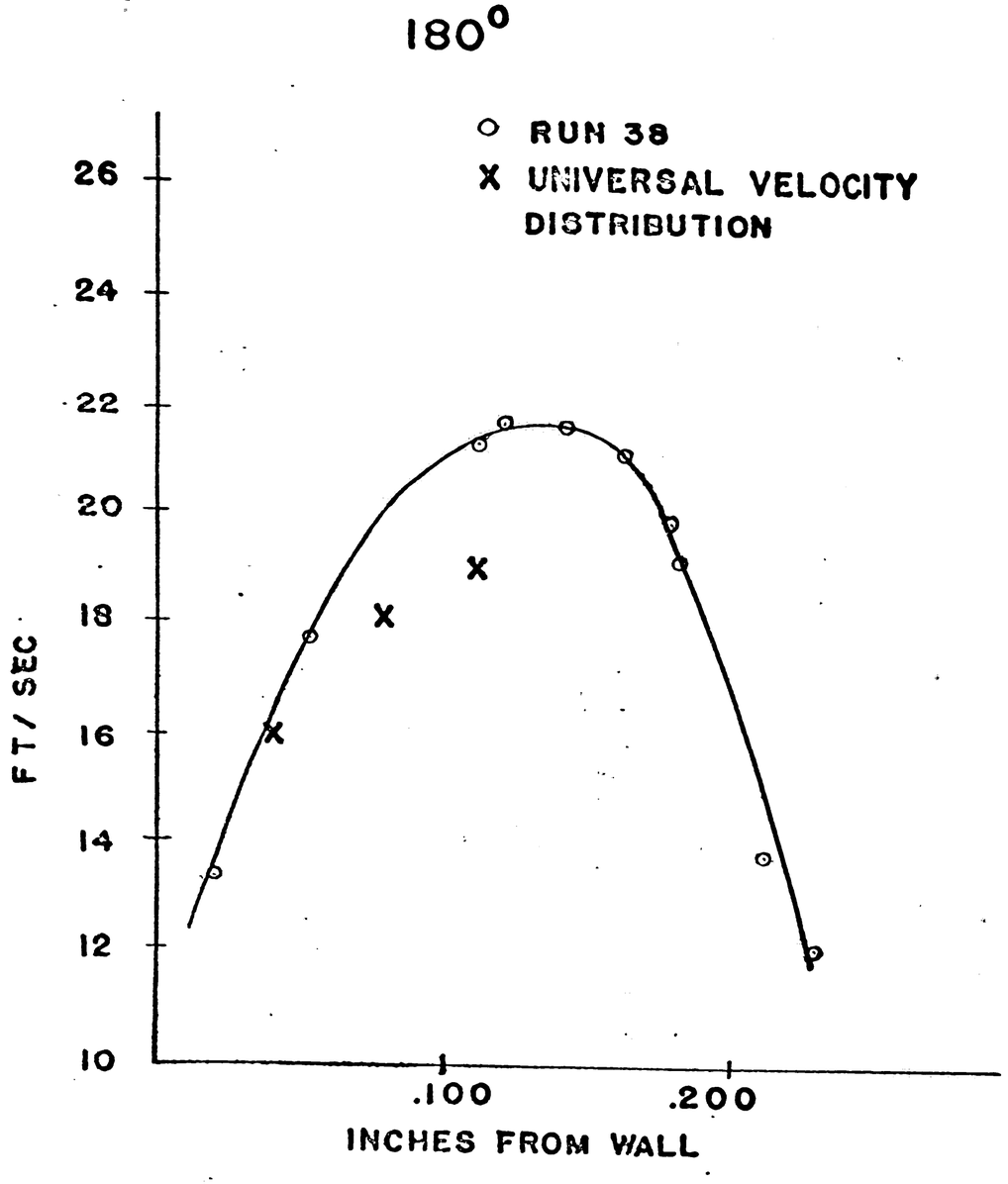

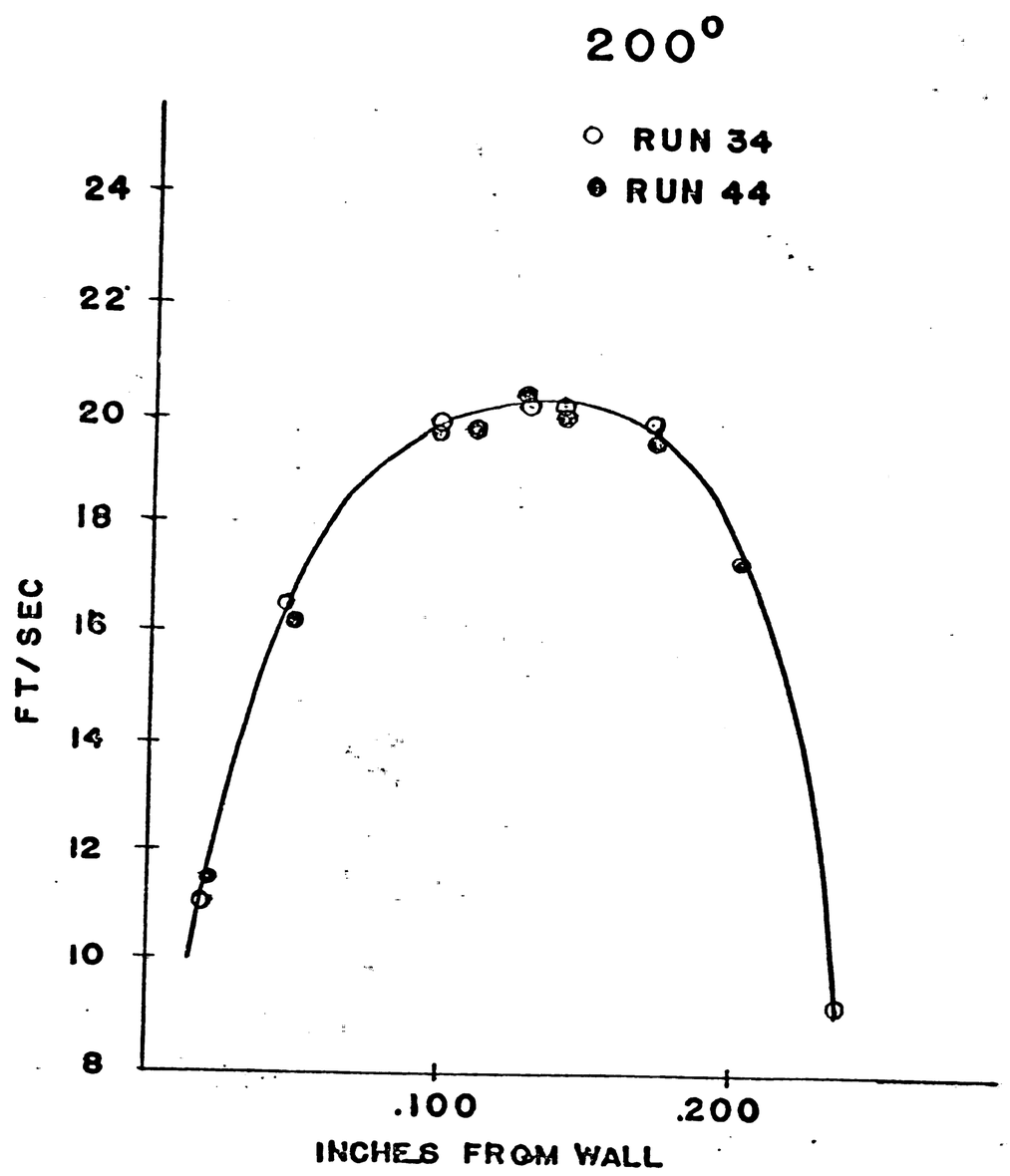

FIGURE 11

VELOCITY PROFILE

240°

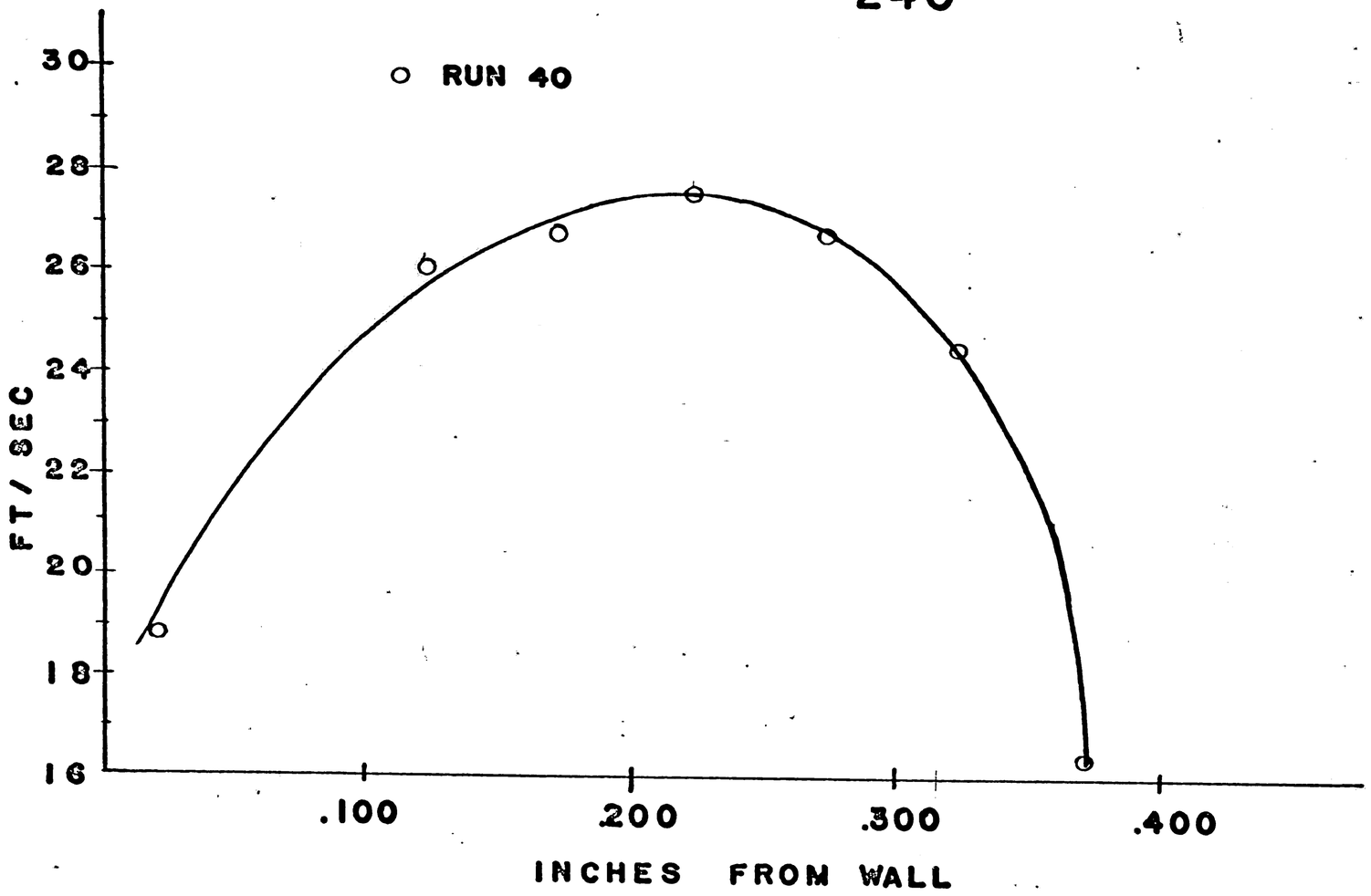

FIGURE 12

the runs except the 1800 traverse where error up to 20 percent was found (see Figures 7 to 12).

C. Determination of Maximum Velocity Points by the Rigorous Solution of the Navier Stokes Equation and by the Noyes Approximation.- As suggested by Heyda the locus of maxima for the laminar flow in the eccentric annulus was calculated using the solution of the Navier Stokes equation in bipolar coordinates (see Appendix B-2). The solution of this equation involved a trial and error procedure which is shown along with the trial calculations in Table . These calculations established maximum points at seven traverse angles as presented in Figure 13. Noyes has suggested that an approximation of the locus of maximum points could be obtained employing a simple formula. The background for the Noyes approximation is presented in Appendix B-1. The locus of points calculated by the Noyes approximation are also presented on Figure 13. The difference between experimentally determined velocity points and those calculated by the Navier Stokes equation and by the Noyes approximation are presented in Table 1. These results tabulated in Table 1 are significant for they show that points of maximum velocity for turbulent flow in an eccentric annulus may be accurately estimated employing either the rigorous Navier Stokes solution or the Noyes approximation equation. The identity of the laminar and turbulent loci also will be of considerable aid in the graphical calculations presented by Deissler and Taylor, for this makes available a very

MAXIMUM VELOCITY IN AN ECCENTRIC ANNULUS

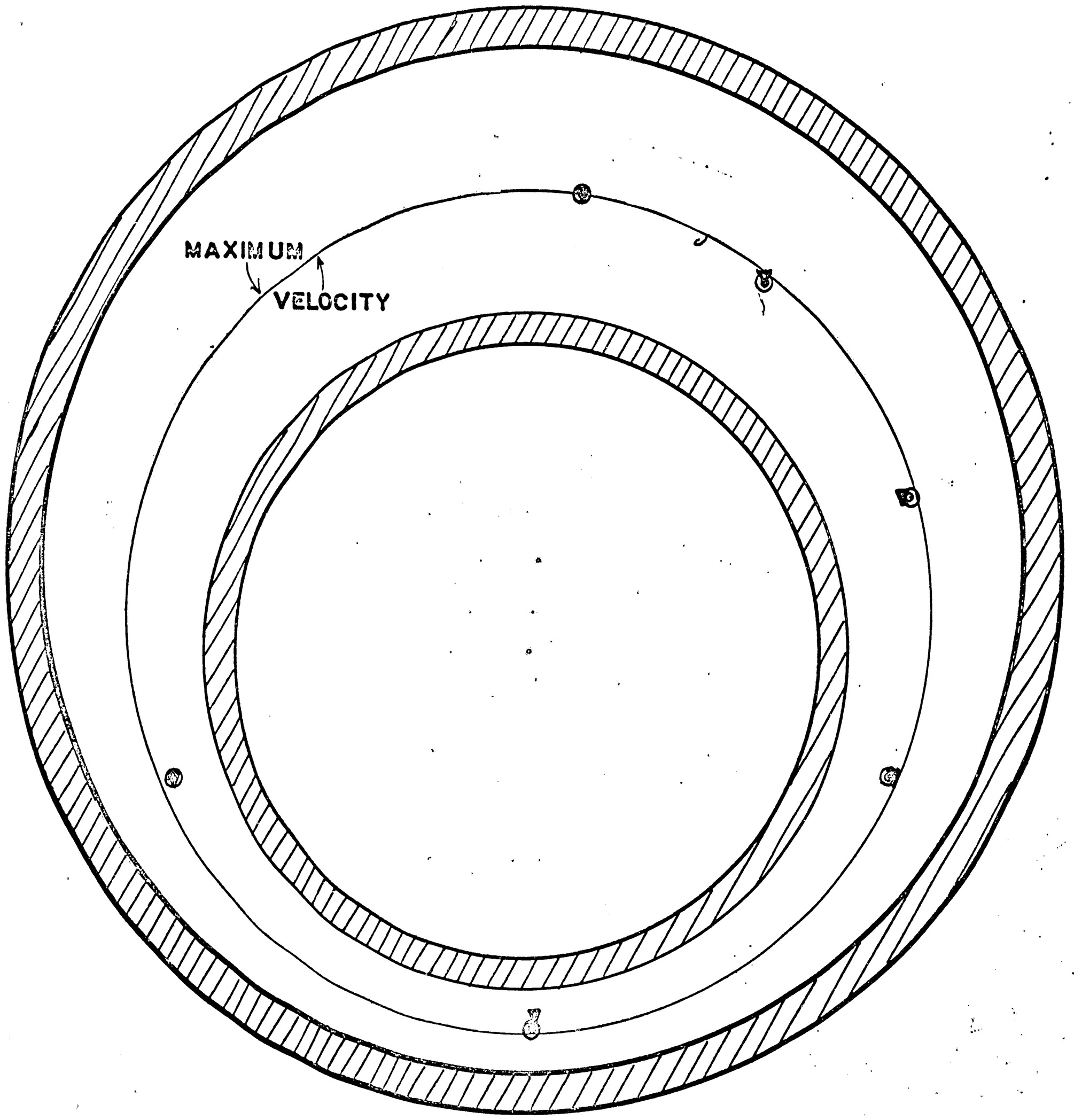

— NOYES APPROXIMATION

RIGOROUS SOLUTION FROM
▼ NAVIER STOKES EQUATION

◎ EXPERIMENTAL POINTS

FIGURE 13

TABLE II

Difference Between Experimentally Determined Maximum Velocity Points And Those Calculated By The Navier Stokes Equation And The Noyes Appoximation Locus

Traverse Angle	η_{exp}	$\eta_{N.S}$ (1)	η_{Noyes} (1)	Error N. S.	Error Noyes
0	1.30	1.32	1.30	2.4	0.0
40	1.30	1.31	1.30	1.8	0.0
80	1.30	1.34	1.30	11.4	0.0
120	1.30	1.29	1.30	6.7	0.0
180	1.29	1.30	1.30	7.2	7.2
200	1.29	1.30	1.30	10.0	10.0
240	1.32	1.28	1.30	14.3	6.6

Note: Error is reported in percent of total traverse distance between points located experimentally and those calculated using the Navier Stokes equation and the Noyes approximation locus.

$\eta_{N.S.}$ from Navier Stokes Equation

η_{NOYES} Noyes Approximation Locus

accurate first approximation of the maxima line and from this the additional graphical approximation of the velocity gradient lines will not be difficult.

Further Work - The relationship between location of the locus and Reynolds number for flow in concentric systems has been investigated by Rothfus (12) and others (7,13,14). It has been reported that the location of the locus is identical for laminar turbulent flow up to 10,000 Reynolds number. At flows greater than 10,000 Reynolds number it is reported that the locus approaches asymptotically some position between the laminar locus and the inner core. It would be interesting to investigate the behavior of the maximum locus as a function of Reynolds number to verify the findings for the concentric systems as general phenomena of annular flow.

In a paper by Redberger and Charles (9), a description of laminar flow variation with eccentricity factors is discussed from the basis of analytical solutions obtained from a digital computer solution of the Navier Stokes Equation. For equal pressure drops a large increase in flow is noted when the eccentricity of the inner core is increased. It would be interesting to develop the same solutions for the turbulent flow case and to develop correlations accurately relating flows to pressure drops as a function of eccentricity factors as done in the above work.

Since the velocity profiles existing in turbulent flow are a function of the so-called eddy diffusivity of momentum, it should

be possible to find expressions for this eddy diffusivity term from the resulting profiles. As has been pointed out by Hinze (6), there are a great number of phenomenological theories which might be used to evaluate the diffusivity term from the data obtainable from an experiment similar to the one reported here.

A P P E N D I C E S

APPENDIX A-1

Solution of Deissler and Taylor- To apply the u^+, y^+ relationships to the calculation of the velocity profiles in an eccentric annulus Deissler and Taylor (3) employed an iterative procedure involving the initial approximation of the location of the line of maximum velocity and the velocity gradient lines. The iterative procedure then involves the calculation of the maximum velocities using the u^+, y^+ relationships calculated in a perpendicular direction from each wall. The resulting velocities for the maximum point are then compared. To apply the universal velocity distribution relationships it is required that the wall stresses be known. Force balances are made on areas, ΔA_1 & ΔA_2, perpendicular to the axial flow and bounded by the physical walls of the system, velocity gradient lines, and the locus of maxima. Referring to Figure 14 the lengths Δl_1 and Δl_2 are chosen so that straight lines drawn normal to them at their midpoints meet at the line of maximum velocity. It is then necessary to match the velocities at the point of intersection on the maximum line using the u^+, y^+ relationships. In order to write force balances on the elements ΔA_1 and ΔA_2 the shear forces acting on Δl_1 and Δl_2, and the pressure forces acting on the faces of the elements must be considered. There are no shear forces acting on the velocity gradient lines, because normal velocity derivatives are zero along these lines. Writing balances on the areas ΔA_1 and ΔA_2

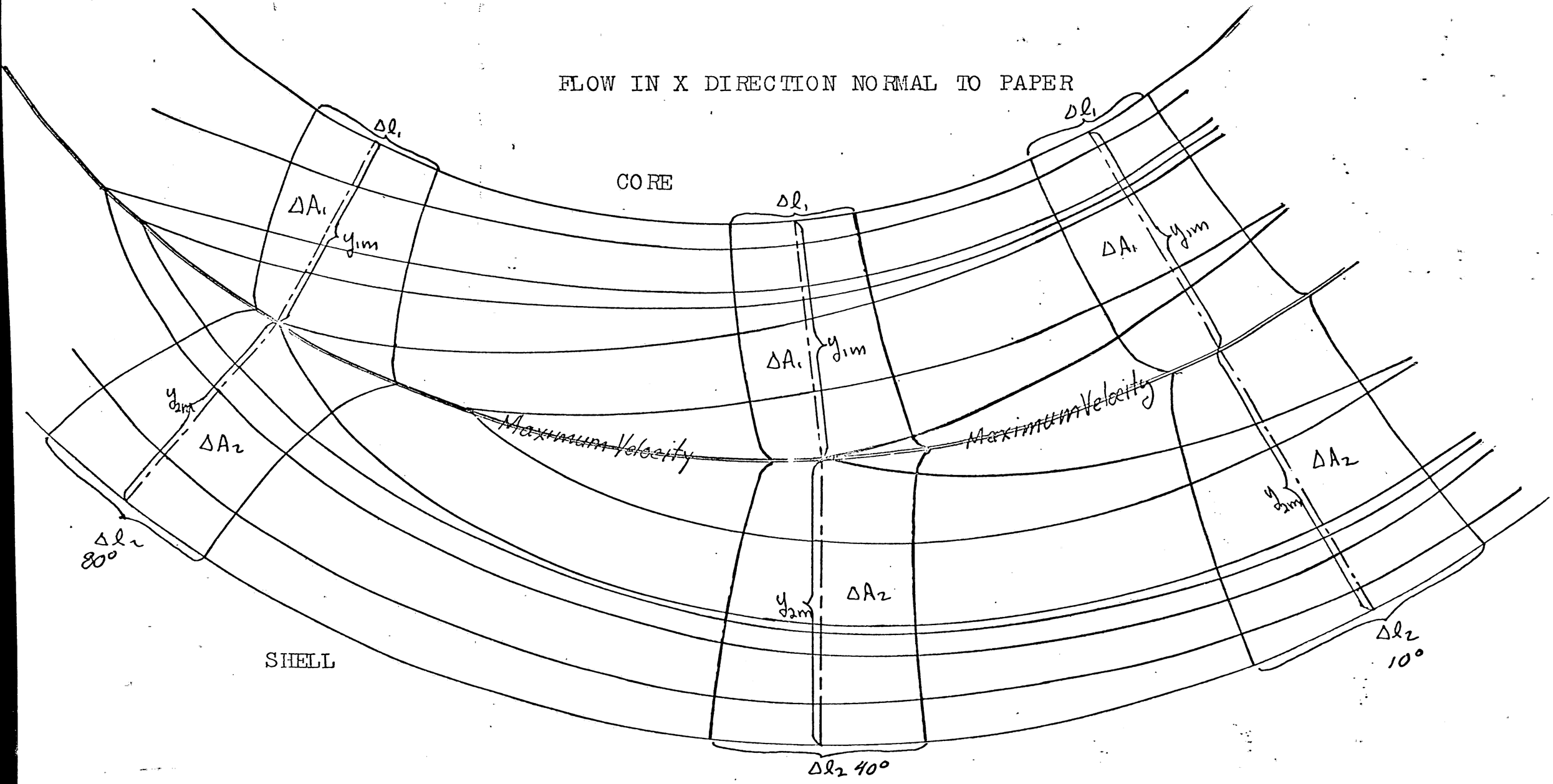

GRAPHICAL DETERMINATION OF VELOCITY PROFILES IN AN ECCENTRIC ANNULUS
BY
THE METHOD OF DEISSLER AND TAYLOR

FIGURE 14

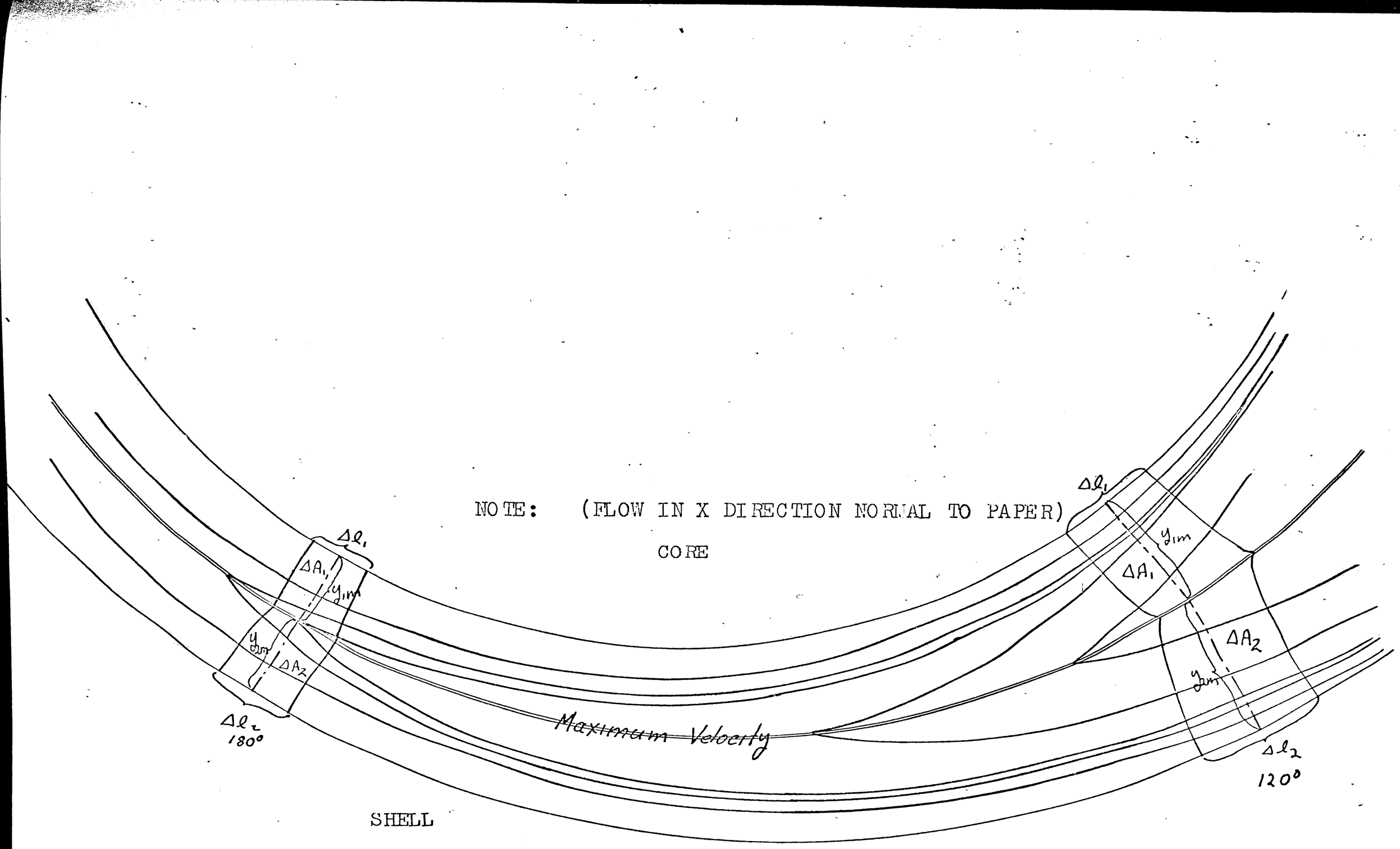

GRAPHICAL DETERMINATION OF VELOCITY PROFILES IN AN ECCENTRIC ANNULUS
BY
THE METHOD OF DEISSLER AND TAYLOR

FIGURE 15

$\tau_1 = -\frac{\Delta A_1}{\Delta \ell_2}\left(\frac{dP}{dx}\right)$ $\tau_2 = -\frac{\Delta A_2}{\Delta \ell_2}\left(\frac{dP}{dx}\right)$ combining these force balances the following results $\tau_2/\tau_1 = \frac{\Delta \ell_1}{\Delta \ell_2} \cdot \frac{\Delta A_2}{\Delta A_1}$

The universal velocity terms are defined as follows $u_i^+ = u_i/\sqrt{\tau_i/\rho}$

$y_i^+ = \frac{\sqrt{\tau_i/\rho}}{\mu/\rho} y_i$ & $u_i^+ = F(y_i^+)$ $\therefore \frac{u_i}{\sqrt{\tau_i/\rho}} = F\left(\frac{\tau_i/\rho}{\mu/\rho} y_i\right)$

and thus $\sqrt{\frac{\tau_1}{\tau_2}} = \frac{F\left(\frac{\sqrt{\tau_1/\rho}}{\mu/\rho} y_{1m}\right)}{F\left(\frac{\sqrt{\tau_2/\rho}}{\mu/\rho} y_{2m}\right)}$ elimination of τ_1 and τ_2 results

in the following $\frac{\sqrt{\frac{\Delta A_2/\Delta \ell_2}{F_1}}}{\sqrt{\frac{\Delta A_1/\Delta \ell_1}{F_1}}} = \frac{F(y_1^+{}_m)}{F(y_2^+{}_m)} = \frac{u_1^+{}_m}{u_2^+{}_m}$

Thus Deissler and Taylor have developed a relationship which enabled them to calculate in an iterative manner the maximum velocity line. Their procedure is to estimate a position of the maximum locus and to approximate the velocity gradient lines. With this assumed profile they can then calculate $u_1^+{}_m$ and u_{2m}^+ and compare the ratio of $u_1^+{}_m/u_2^+{}_m$ to that of $\sqrt{\frac{\Delta A_2/\Delta \ell_2}{F_1}}\Big/\sqrt{\frac{\Delta A_1/\Delta \ell_1}{F_1}}$. If agreement does not result a new position for the maximum locus is established and new gradient lines drawn.

In the calculations performed here the maxima line was first taken to be that defined from the maxima measured in the experiment. Figures 14 and 15 show the enlarged construction of the maxima locus and the gradient lines for the traverses made at 10°, 40°, 80°, 120°, and 180 degrees. The areas and lengths measured from these drawings are presented in Table 2. All areas were accurately determined with a planimeter. To

calculate the velocity profiles from the outer shell to the locus of maxima, the normal velocity distribution method was followed (as outlined below).

APPENDIX A-2

Sample Calculation of Point Velocities and Maximum Point by the Method of Deissler and Taylor.

Evaluation of System Constants-

1) Kinematic viscosity $\mu/\rho = \nu$ Temp. 106°F

$$\mu = .0185\,cp \times 2.09\times10^{-5} \frac{\#f\text{-}sec/ft^2}{cp} = 3.866\times10^{-7} \frac{\#f\text{-}sec}{ft^2}$$

$$\rho = 7.04\times10^{-2} \frac{\#m}{ft^3} \times \frac{1\,\#f\,sec^2}{32.2\,\#m\,ft} = 2.19\times10^{-3} \frac{\#f\,sec^2}{ft^4}$$

$$\nu = \mu/\rho = \frac{3.866\times10^{-7}\ \#f\text{-}sec/ft^2}{2.19\times10^{-3} \frac{\#f\,sec^2}{ft^4}} = 1.76\times10^{-4} \frac{ft^2}{sec}$$

2) Axial Pressure Drop dP/dL

$$\frac{dP}{dL} = \frac{\rho \Delta z\, g/g_c}{\Delta L} = \frac{60.5 \frac{\#m}{ft^3} \times .06 \frac{in}{12in} \times 1ft \times \frac{\#f}{\#m}}{1\ ft} = 0.3025 \frac{\#f}{ft^2 \cdot ft}$$

Sample Calculations For 40° Traverse Runs 41, 36, &45-

From Figure

$y_{1m} = 0.349''$ $\quad y_{2m} = 0.412''$

$\Delta l_1 = 0.164''$ $\quad \Delta l_2 = 0.300''$

$\Delta A_1 = 0.0656''^2$ $\quad \Delta A_2 = 0.106''^2$

$$\gamma_1 = -\frac{\Delta A_1}{\Delta l_1}\left(\frac{dP}{dL}\right) = \frac{.0656''^2}{0.164''} \times \frac{1ft}{12''} \times .3025 \frac{\#f}{ft^2 \cdot ft} = 1.02\times10^{-2} \frac{\#f}{ft^2}$$

$$\gamma_2 = -\frac{\Delta A_2}{\Delta l_2}\left(\frac{dP}{dL}\right) = \frac{.106''^2}{.300''} \times \frac{1ft}{12''} \times .3025 \frac{\#f}{ft^2 \cdot ft} = 0.890\times10^{-2} \frac{\#f}{ft^2}$$

$\frac{\tau_1}{\rho} = \frac{1.02 \times 10^{-2} \#f/ft^2}{2.19 \times 10^{-3} \frac{\#f sec^2}{ft^4}} = 4.61 \frac{ft^2}{sec^2}$ $\quad \frac{\tau_2}{\rho} = \frac{0.890 \times 10^{-2} \frac{\#f}{ft^2}}{2.19 \times 10^{-3} \frac{\#f sec^2}{ft^4}} = 4.06 \frac{ft^2}{sec^2}$

$\sqrt{\frac{\tau_1}{\rho}} = \sqrt{4.61} \frac{ft}{sec} = 2.15 \frac{ft}{sec}$ $\quad \sqrt{\frac{\tau_2}{\rho}} = \sqrt{4.06} \frac{ft}{sec} = 2.02 \frac{ft}{sec}$

$y_{1m}^+ = \frac{\sqrt{\tau_1/\rho}}{\mu/\rho} y_{1m} = \frac{2.15 ft/sec \times 1ft/12" \times .349"}{.8025 \frac{\#f}{ft^2 ft}} = 355$

$y_{2m}^+ = \frac{\sqrt{\tau_2/\rho}}{\mu/\rho} y_{2m} = \frac{2.02 ft/sec \times 1ft/12" \times .412"}{.3025 \frac{\#f}{ft^2 ft}} = 394$

$u_i^+ = 2.78 \ln y_i^+ + 3.8$

$u_{1m}^+ = 2.78 \ln 355 + 3.8 = 20.1$

$u_{2m}^+ = 2.78 \ln 394 + 3.8 = 20.4$

To Check: $\frac{\sqrt{\frac{\Delta A_2/\Delta l_2}{r_1}}}{\sqrt{\frac{\Delta A_1/\Delta l_1}{r_1}}}$ should $\cong \frac{u_1^+m}{u_2^+m}$

$\frac{\sqrt{\frac{.106}{.3 \times 1}}}{\sqrt{\frac{.0656}{.164 \times 1}}} = 0.938$ $\quad \frac{u_1^+m}{u_2^+m} = \frac{20.1}{20.4} = .985$

Calculation of Maximum Velocity:

$u_1^+m = \frac{u_{1m}}{\sqrt{\tau_1/\rho}}$ $\quad u_{1m} = 20.1 \times 2.15 = 43.2$ ft/sec

$u_2^+m = \frac{u_{2m}}{\sqrt{\tau_2/\rho}}$ $\quad u_{2m} = 20.4 \times 2.02 = 41.6$ ft/sec

Ave. of u_{1m} & u_{2m} = 42.4 ft/sec

Expt value of u_{max} = 41.2 ft/sec

Calculation of Velocity Profile from Shell to Maxima

$y_2^+ = \frac{y_2}{y_{2m}} y_{2m}^+$

Distance from Shell	y_2^+	u_2^+	u(ft/sec)
0.100"	95.7	16.5	33.3
0.200"	191	18.4	37.2
0.300"	287	19.5	39.4
0.400"	383	20.3	41.0

Points calculated from the inner core using this method are not on the same traverse as the experimentally measured points. Therefore, they are not calculated since comparison can not be made.

Table 2

Dimensions Of Segments Bounded By The Maximum Locus, Velocity Gradient Lines, And The Walls Of The Annulus - As Shown In Figures 13 and 14.

Traverse Angle	y_{1m}	Δl_1	ΔA_1	y_{2m}	Δl_2	ΔA_2
10^0	.362"	.190"	$.0772"^2$	.437"	.380"	$.134"^2$
40^0	.349"	.164"	$.0656"^2$	.412"	.300"	$.106"^2$
80^0	.335"	.190"	$.0560"^2$	.297"	.282"	$.0816"^2$
120^0	.200"	.160"	$.0360"^2$	.238"	.200"	$.0416"^2$
180^0	.122"	.095"	$.0128"^2$	.133"	.125"	$.0160"^2$

TABLE 3

Terms Employed In the Determination Of Maximum Velocity Points

By The Method Of Deissler And Taylor

Traverse Angle	i	$\frac{\Delta A_i}{\Delta l_i}$	$\tau_i \times 10^2$	τ_i/ρ	$\sqrt{\frac{\tau_i}{\rho}}$	y_{im}	y^+_{im}	u^+_{im}
10	1	.406	1.020	4.66	2.16	.362	370	20.2
10	2	.353	0.809	4.06	2.02	.437	418	20.6
40	1	.400	1.010	4.61	2.15	.349	355	20.1
40	2	.353	0.890	4.06	2.02	.412	394	20.4
80	1	.295	0.743	3.39	1.84	.297	259	19.2
80	2	.289	0.728	3.32	1.82	.335	289	19.6
120	1	.225	0.567	2.59	1.61	.200	152	17.8
120	2	.208	0.524	2.39	1.55	.238	175	18.1
180	1	.135	0.340	1.55	1.24	.122	72	15.7
180	2	.128	0.322	1.47	1.21	.133	76	15.8

Traverse Angle	i	$\sqrt{\frac{\Delta A_i/\Delta l_i}{r_1}}$	$\sqrt{\frac{\Delta A_2/\Delta l_2}{r_1}} \Big/ \sqrt{\frac{\Delta A_1/\Delta l_1}{r_1}}$	$\frac{u^+_{1m}}{u^+_{2m}}$	u_{im}	u experimental
10	1	.637	.932	.981	43.6	
10	2	.594			41.6	
40	1	.633	.938	.985	43.2	42.0
40	2	.594			41.6	
80	1	.544	.989	.980	35.3	36.0
80	2	.538			35.7	
120	1	.474	.962	.983	28.6	27.6
120	2	.456			28.0	
180	1	.368	.973	.994	19.6	21.8
180	2	.358			19.2	

TABLE 4

Determination Of Velocity Profiles By The Method Of Deissler And Taylor

Traverse Angle	Distance of Point from Shell	y_2^+	u_2^+	u_2 (ft/sec)
40	0.100"	95.7	16.5	33.3
	0.200"	191	18.4	37.2
	0.300"	287	19.5	39.4
	0.400"	383	20.3	41.0
80	0.100"	85.8	16.2	29.5
	0.150"	129	17.3	31.5
	0.200"	172	18.1	32.9
	0.250"	215	18.7	34.0
	0.300"	258	19.2	34.9
120	0.050"	36.8	13.8	21.4
	0.100"	73.5	15.8	24.5
	0.150"	110	16.9	26.2
	0.200"	147	16.7	27.4
	0.230"	169	18.1	28.0
180	0.050"	28.6	13.1	15.8
	0.100"	57.1	15.0	18.2
	0.130"	74.2	15.8	19.2

APPENDIX B-1

Solution of the Navier Stokes equation for the locus maximum velocity in an eccentric annulus. To solve the Navier Stokes equation for the geometrical configuration of the eccentric annulus Heyda(5) employed the bipolar coordinate system. Before Heyda's solution is considered the bipolar coordinate system will be discussed and the system investigated in this report will be defined in bipolar coordinate terms.

The bipolar coordinate system consists of sets of orthogonal circles. As shown in Figure 16 below a point in the

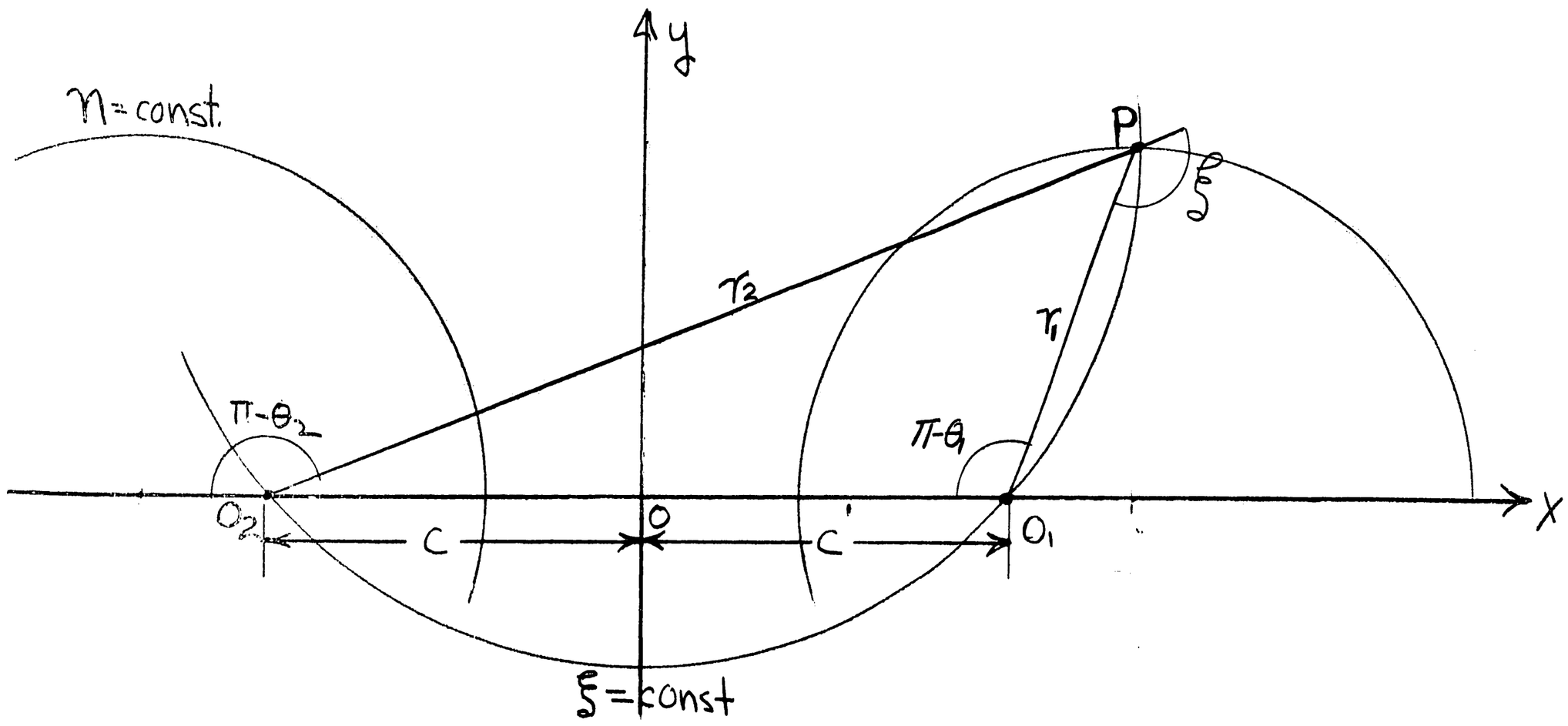

Figure 16 Bipolar Coordinate System

x-y plane may be located specifying the circles having centers on the x and y axis which intersect at P. To define the specific circles it is noted that the circle with its center on the y axis has the property that any point on its circumference creates a

a constant angle $\theta_1 - \theta_2$ and thus this circle is defined as $\xi = \pi - (\theta_1 - \theta_2)$ constant circle. The circles having their centers on the x-axis are orthogonal to the y-axis circle and have the property that $\ln \frac{r_1}{r_2} = \eta$, a constant. Thus the point P is defined in terms of the ξ and η circles.

To apply this coordinate system to the problem of interest it will be advantageous to consider the x-y plane as the complex z plane and to define a new complex plane $\omega = \xi + i\eta$. To determine the transformation between the z and ω planes implied by the bipolar relations above observe that

$$\frac{r_1}{r_2} = e^{\eta} = \frac{|\vec{PO} + \vec{OO_1}|}{|\vec{O_2O} + \vec{OP}|} = \frac{|c - z|}{|c + z|} \quad \text{or} \quad e^{-\eta} = \left|\frac{c+z}{c-z}\right| \qquad (1)$$

$$\xi = \theta_2 - (\theta_1 - \pi) = \arg(c+z) - \arg(c-z) = \arg\left(\frac{c+z}{c-z}\right) \qquad (2)$$

Hence ξ and $e^{-\eta}$ are respectively the angle and the absolute value of the complex variable $\mathcal{L} = \frac{c+z}{c-z}$ (3) writing in polar form

$$\mathcal{L} = \rho e^{i\xi} \qquad \rho = e^{-i\eta}$$

$$\mathcal{L} = e^{-\eta + i\xi} = \frac{c+z}{c-z} \qquad (4)$$

$$z = ic \tan(1/2\omega) \qquad (5)$$

It can be seen from equation (3) above that in the $\mathcal{L}$-plane, the circle $|\xi| = \rho$ is the map of the circle $\left|\frac{c+z}{c-z}\right| = \rho$; which, in the z plane has its center at $\left[-c\left(\frac{1+\rho^2}{1-\rho^2}\right), 0\right]$ and is of radius $\frac{2c\rho}{1-\rho^2}$.

Since $\rho = e^{-\eta}$, the center and radius may be compactly written as $[-c\coth\eta, 0]$ and $c\operatorname{csch}\eta$. In Figure 17, A and B are characterized by η_1 & η_2 respecitvely, then $a = c\operatorname{csch}\eta_1$ and $b = c\operatorname{csch}\eta_2$.

Denoting the distance between the centers of A and B by d

$$d = c(\coth\eta_2 - \coth\eta_1)$$

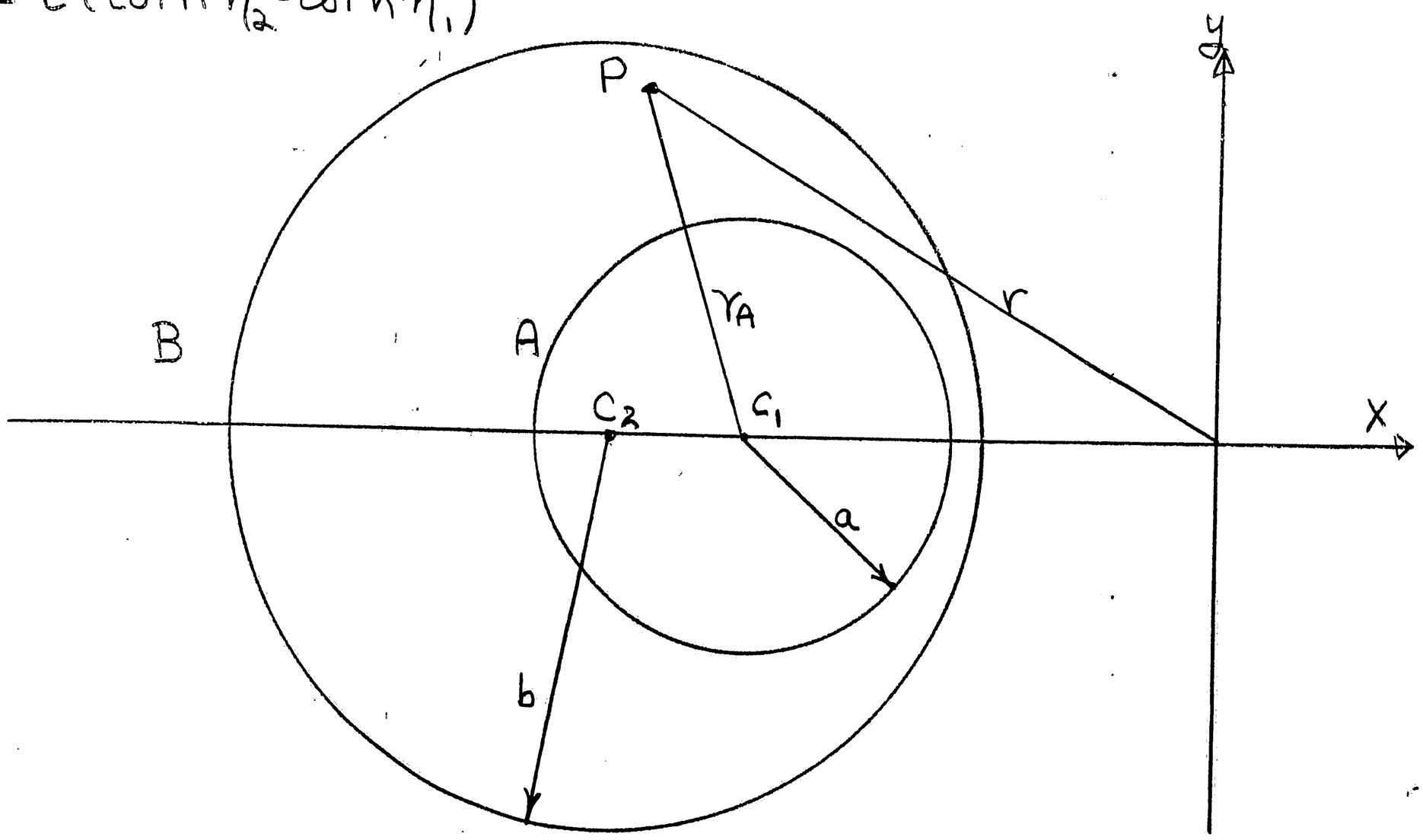

Figure 17 Eccentric Annulus

It is convenient to define the eccentricity ε and a radius S ratio as follows $\varepsilon = \frac{d}{b-a}$ and $S = \frac{a}{b}$. Then it may be shown that

$$2\cosh\eta_2 = \frac{1+S}{\varepsilon} + (1-S)\varepsilon \qquad c = b\sinh\eta_2$$

$$\sinh\eta_1 = c/a$$

With the bipolar coordinate system defined above its use will be illustrated by placing the system investigated in the bipolar coordinates.

$a = 1.0''$
$b = 1.53''$
$d = 0.27''$
} physical dimensions of system

$$S = a/b = 1.0/1.53 = 0.65$$

$$\varepsilon = d/b-a = \frac{.27}{1.53-1.00} = 0.51$$

$$2\cosh\eta_2 = \frac{1+S}{\varepsilon} + (1-S)\varepsilon$$

$$2\cosh\eta_2 = \frac{1+.65}{.51} + (.35)(.51) = 3.42$$

$$\eta_2 = 1.13$$

$b = c\,\mathrm{csch}\,\eta_2 \qquad c = b \sinh \eta_2 = 1.53 \times 1.386 = 2.12$

$\sinh \eta_1 = c/a = 2.12 \qquad \eta_1 = 1.50$

summarizing: $a = 1.00 \qquad c = 2.12$

$b = 1.53 \qquad \eta_1 = 1.50$

$d = 0.27 \qquad \eta_2 = 1.13$

To define completely the system the center of one of the circles must be found. As above $\eta_{2_{center}} = [c \coth \eta_2, 0]$ and $\eta_{2_{center}} = 2.615$. With this information the system is placed in bipolar coordinates as shown in Figure 18.

Figure 18 Experimental Eccentric Annulus in Bipolar Coordinates.

Solution Of The Navier Stokes Equation For Point Velocities Of Turbulent Flow In An Eccentric Annulus - For fully developed laminar flow of an incompressible fluid of viscosity μ

$$\nabla^2 v(x,y) = -\frac{1}{\mu}\frac{dP}{dL} \qquad (1)$$

with boundary conditions that v=0 on circles A and B. A solution of equation (1) with v=0 on A but not on B can be verified to be $v_1 = -\frac{1}{4\mu}\frac{dP}{dL}\left(r_A^2 - a^2\right)$ where a is the radius of circle A on center C_1, and $r_A = C_1P$.

To satisfy both equation (1) and both boundary conditions a second solution must be found which vanishes on A, and which assumes a value of $v_2 = -v_1$ on B. In the following development the functions v_1 and v_2 will be found in bipolar coordinates so that $v(\xi,\eta) = v_1 + v_2$.

Referring to Figure 17 and applying the law of sines

$(a^2 = b^2 + c^2 - 2bc\cos A)$ $\quad r_A^2 = r^2 + (c\coth\eta)^2 + 2r(c\coth\eta_1)\cos\theta$

then since $a = c\,\mathrm{csch}\,\eta_1$

$$r_A^2 - a^2 = c^2\coth^2\eta_1 - c^2\,\mathrm{csch}^2\eta_1 + \coth\eta_1(2rc\cos\theta) + r^2$$
$$= r^2 + c^2 - \coth\eta_1(-2rc\cos\theta)$$

It can be shown by transformation that $\tanh\eta = -\frac{2cr\cos\theta}{r^2+c^2}$.

Therefore $r_A^2 - a^2 = r^2 + c^2 - (r^2+c^2)\coth\eta_1\tanh\eta$

and $v_1 = -\frac{1}{4\mu}\frac{dP}{dL}(r^2+c^2)[1 - \coth\eta_1\tanh\eta]$ $\quad (\because v_1 = 0 \text{ @ } \eta = \eta_1)$

To find the second solution Heyda (5) notes that v_2 is a harmonic function of x,y since it satisfies the equation $\nabla^2 v_2 = 0$. Since the transformation function $\zeta = \frac{c+z}{c-z}$ is analytic v_2 is also a harmonic function in terms of the variables ρ and ξ.

By transformation of coordinates Laplace's equation becomes

$$\frac{\partial^2 v_2}{\partial \rho^2} + \frac{1}{\rho}\frac{\partial v_2}{\partial \rho} + \frac{1}{\rho^2}\frac{\partial^2 v_2}{\partial \xi^2} = 0$$

Upon separating variables and noting that v_2 must be an even function of ξ Heyda finds that $v_2 = A_0 \ln\rho + B_0 + \sum_{n=1}^{\infty}(A_n\rho^n + B_n\rho^{-n})\cos n\xi$

In order for the function v_2 to vanish on circle A, i.e., when $\rho=\rho_1$, it is necessary that $A_0 \ln\rho_1 + B_0 = 0$ $A_n\rho_1^n = -B_n\rho_1^{-n}$ $n=1,2,3\ldots$

then $B_0 = -A_0 \ln\rho_1$ $B_n = -A_n\rho_1^{2n}$ $n=1,2,3\ldots$

Then changing the definition of A_n $v_2 = A_0 \ln\frac{\rho}{\rho_1} + \sum_{n=1}^{\infty}\frac{A_n}{2}\left[\left(\frac{\rho}{\rho_1}\right)^n - \left(\frac{\rho}{\rho_1}\right)^{-n}\right]\cos n\xi$

Since $\rho = e^{-\eta}$ this expression can be rewritten in the more manageable form $v_2 = -A_0(\eta-\eta_1) + \sum_{n=1}^{\infty} A_n \sinh n(\eta_1-\eta)\cos n\xi$

To evaluate the requisite constants the equation $v_1 + v_2 = 0$ at $\eta=\eta_2$ is investigated $-A_0(\eta_2-\eta_1) + \sum_{n=1}^{\infty} A_n \sinh n(\eta_1-\eta)\cos n\xi =$

$$\frac{1}{4\mu}\frac{dP}{dL}\left(r^2_{\eta=\eta_2} + C^2\right)(1-\coth\eta_1\tanh\eta_2) \qquad (2)$$

To aid in this evaluation an expansion for r_2 in terms of ξ and η is needed. In reference (5), using the method of residues, the following expression is obtained

$$\frac{1}{\cosh\eta+\cos\xi} = \frac{1}{\sinh\eta}\left[1 + 2\sum_{n=1}^{\infty}(-1)^n e^{-n\eta}\cos n\xi\right]$$

It can be shown that $r_2 + C_2 = C^2(2\cosh\eta/\cosh\eta+\cos\xi)$

$$\therefore r^2 + C^2 = 2C^2\coth\eta\left[1 + 2\sum_{n=1}^{\infty}(-1)^n e^{-n\eta}\cos n\xi\right]$$

Then the right hand side of (2) above may be rewritten as follows $\frac{1}{4\mu}\frac{dP}{dL}\cdot 2C^2\coth\eta_2\left[1 + 2\sum_{n=1}^{\infty}(-1)^n e^{-n\eta}\cos n\xi\right]\left[1-\coth\eta,\tanh\eta\right]$

$$= \frac{1}{4\mu}\frac{dP}{dL}2C^2(\coth\eta - \coth\eta_1)\left[1 + 2\sum_{n=1}^{\infty}(-1)^n e^{-n\eta}\cos n\xi\right]$$

$$= \frac{1}{4\mu}\frac{dP}{dL}2cd\left[1 + 2\sum_{n=1}^{\infty}(-1)^n e^{-n\eta}\cos n\xi\right]$$

Equating terms $A_0 = \frac{-Kcd}{2(\eta_2-\eta_1)}$ $K = \frac{1}{\mu}\frac{dP}{dL}$ $A_n = \frac{(-1)^n Kcd\, e^{-n\eta_2}}{\sinh n(\eta_1-\eta_2)}$ $n = 1, 2, 3, \ldots$

Placing these new constants in the expression for v_2

$$v_2 = \frac{Kcd}{2}\left(\frac{\eta-\eta_2}{\eta_1-\eta_2}\right) + Kcd\sum_{n=1}^{\infty}(-1)^n e^{-n\eta_2}\frac{\sinh n(\eta_1-\eta)}{\sinh n(\eta_1-\eta_2)}\cos n\xi$$

Adding the solutions v_1 and v_2 the desired expression results

$$v(\xi,\eta) = \frac{1}{4\mu}\frac{dP}{dL}\left[-\frac{2c^2\cosh\eta(1-\coth\eta_1\tanh\eta)}{\cosh\eta+\cos\xi} + 4Kcd\sum_{n=1}^{\infty}\frac{e^{-n\eta_2}\sinh n(\eta_1-\eta)\cos n\xi}{\sinh n(\eta_1-\eta_2)} + 2Kcd\left(\frac{\eta_1-\eta}{\eta_1-\eta_2}\right)\right] \quad (3)$$

To obtain the line of maximum velocity $\frac{dv}{d\eta}$ is set equal to zero for each ξ. To perform this manipulation equation (3) is differentiated term by term below

$$\frac{d}{d\eta}\left[\frac{-2c^2\cosh\eta(1-\coth\eta_1\tanh\eta)}{\cosh\eta+\cos\xi}\right] = -2c^2\frac{d}{d\eta}\left[\frac{\cosh\eta-\coth\eta_1\sinh\eta}{\cosh\eta+\cos\xi}\right]$$

$$= -2c^2\left\{\frac{(\cosh\eta+\cos\xi)(\sinh\eta-\coth\eta_1\cosh\eta) - \sinh\eta(\cosh\eta-\coth\eta_1\sinh\eta)}{(\cosh\eta+\cos\xi)^2}\right\}$$

$$= -2c^2\left\{-\frac{\frac{\cosh\eta_1}{\sinh\eta_1} + \cos\xi\left(\frac{\sinh\eta\sinh\eta_1 - \coth\eta\cosh\eta_1}{\sinh\eta_1}\right)}{(\cosh\eta+\cos\xi)^2}\right\}$$

$$= \frac{+2c^2}{\sinh\eta_1}\left\{\frac{\cosh\eta_1+\cos\xi\cosh(\eta_1-\eta)}{(\cosh\eta\cos\xi)^2}\right\} \qquad \text{note: } \sinh\eta_1 = \frac{c}{a}$$

$$= 2ca\left\{\frac{\cosh\eta_1+\cos\xi\cosh(\eta_1-\eta)}{(\cosh\eta+\cos\xi)^2}\right\}$$

$$\frac{d}{d\eta}\left[4Kcd\sum_{n=1}^{\infty}(-1)^n e^{-n\eta_2}\frac{\sinh n(\eta_1-\eta)}{\sinh n(\eta_1-\eta_2)}\cos n\xi\right]$$

$$= 4Kcd\sum_{n=1}^{\infty}(-1)^n e^{-n\eta_2}\frac{\cos n\xi}{\sinh n(\eta_1-\eta_2)}\frac{d}{d\eta}\left[\sinh n(\eta_1-\eta)\right]$$

$$= -4Kcd\sum_{n=1}^{\infty}(-1)^n e^{-n\eta_2}\frac{n\cosh n(\eta_1-\eta)}{\sinh n(\eta_1-\eta_2)}\cos n\xi$$

$$\frac{d}{d\eta}\left[2cd\left(\frac{\eta_1-\eta}{\eta_1-\eta_2}\right)\right] = -\frac{2cd}{\eta_1-\eta_2}$$

If $\frac{\partial V}{\partial \eta} = 0$ then

$$\frac{\cosh\eta_1+\cos\xi\cosh(\eta_1-\eta)}{(\cosh\eta+\cos\xi)^2} = \frac{d}{a}\left[\frac{1}{\eta_1-\eta_2}+2\sum_{n=1}^{\infty}(-1)^n\frac{e^{-n\eta}-e^{n\eta}\cosh n(\eta_1-\eta)\cos n\xi}{\sinh n(\eta_1-\eta_2)}\right] \quad (4)$$

APPENDIX B-2

Calculations Of Maximum Velocity Points By The Methods Of Noyes And Heyda.

Calculation of η_{MAX} by the rigorous solution of the Navier Stokes equation.- A plot of the difference between the right and left side of equation (4) above as a function of η at a set ξ yields the value of η_{MAX} when the difference becomes zero.

Table 5 is a tabulation of the values of η and ξ determined from the experimental measurements. Table 6 presents in tabular form all the data required for the solution of (4) and also presents the resulting differences for each η at a specified ξ.

From this data a plot of Δ vs. η is constructed (see Figure 19) and the values of η max determined (see Table).

Table 5 Experimental Values of η and ξ

Traverse x	V_1	V_2	η	θ_1	θ_2	ξ
0	33.8	8.98	1.32	178	8	10
40	35.9	9.37	1.34	170	41	51
80	42.7	11.5	1.31	165	84	99
120	51.2	13.8	1.31	167	122	135
160	58.6	16.1	1.29	179	175	176
200	58.2	16.1	1.29	176	167	171
240	53.1	14.4	1.30	168	132	144

TABLE 6 Evaluation of $\Delta^{(2)}$

Value of n →	1	2	3	4	5	6	
$\sinh n(\eta_1-\eta_2)$	0.378	0.809	1.352	2.083	3.101	4.549	
$n \cdot e^{-n\eta_2}$	0.323	0.208	0.101	0.044	0.018	0.008	η
$\cosh n(\eta_1-\eta)$	1.039	1.161	1.374	1.696	2.151	2.776	1.22
	1.029	1.117	1.270	1.497	1.811	2.229	1.26
	1.020	1.081	1.186	1.337	1.543	1.811	1.30
	1.013	1.052	1.117	1.212	1.337	1.497	1.34
$(-1)^n e^{-n\eta_2}\times$	-.888	0.298	-.103	.0358	-.0125	.0049	1.22
	-.879	0.287	-.095	.0316	-.0105	.0039	1.26
$\frac{\cosh n(\eta_1-\eta)}{\sinh n(\eta_1-\eta_2)}$	-.871	0.278	-.089	.0282	-.0090	.0032	1.30
	-.866	0.270	-.083	.0256	-.0075	.0026	1.34

Traverse χ							
0°	0.985	0.940	0.866	0.766	0.643	0.500	$\cos n\chi$
40°	0.629	-.208	-.891	-.914	-.259	0.970	
80°	-.156	-.951	0.920	0.242	-.996	-.695	
120°	-.707	0.000	0.707	1.000	-.707	0.000	
180°	-.997	0.990	-.978	0.961	-.940	0.914	
200°	-.988	0.951	-.891	0.809	-.707	0.588	
240°	-.809	0.848	0.309	-.809	1.000	-.809	

Traverse χ →	0°	40°	80°	120°	180°	200°	240°	
1) $\cos\chi\cosh(\eta_1-\eta)$	1.023	0.654	-.162	-.734	-1.036	-1.026	-.840	
2) $\cosh\eta_1+(1)$	3.375	3.006	2.190	1.618	1.316	1.326	1.512	
3) $\cosh\eta+\cos\chi$	2.826	2.470	1.685	1.134	0.844	0.853	1.032	$\eta=1.22$
4) $(3)^2$	7.986	6.101	2.839	1.286	0.712	0.728	1.065	
5) $(2)\div(4)$	0.423	0.493	0.771	1.258	1.848	1.821	1.420	
1) $\cos\chi\cosh(\eta_1-\eta)$	1.014	0.647	-.160	-.728	-1.026	-1.017	-.832	
2) $\cosh\eta_1+(1)$	3.366	2.999	2.192	1.624	1.326	1.335	1.520	
3) $\cosh\eta+\cos\chi$	2.889	2.533	1.748	1.197	0.907	0.916	1.095	$\eta=1.26$
4) $(3)^2$	8.346	6.416	3.056	1.433	0.823	0.839	1.199	
5) $(2)\div(4)$	0.403	0.467	0.717	1.133	1.611	1.591	1.268	
1) $\cos\chi\cosh(\eta_1-\eta)$	1.000	0.642	-.159	-.721	-1.017	-1.008	-.825	
2) $\cosh\eta_1+(1)$	3.352	2.994	2.193	1.631	1.335	1.344	1.527	
3) $\cosh\eta+\cos\chi$	2.956	2.600	1.815	1.264	0.974	0.983	1.162	$\eta=1.30$
4) $(3)^2$	8.738	6.760	3.294	1.598	0.949	0.966	1.350	
5) $(2)\div(4)$	0.384	0.443	0.666	1.021	1.407	1.391	1.131	
1) $\cos\chi\cosh(\eta_1-\eta)$	0.998	0.637	-.158	-.716	-1.001	-1.000	-.820	
2) $\cosh\eta_1+(1)$	3.350	2.989	2.194	1.636	1.351	1.352	1.532	
3) $\cosh\eta+\cos\chi$	3.025	2.669	1.884	1.333	1.043	1.052	1.231	$\eta=1.34$
4) $(3)^2$	9.151	7.124	3.549	1.777	1.088	1.107	1.515	
5) $(2)\div(4)$	0.366	0.420	0.618	0.921	1.242	1.221	1.011	

TABLE 6 (continued)

$$\frac{(-1)^n n \cdot e^{-n\eta_2} \cosh n(\eta_1-\eta)\cos n\xi}{\sinh n(\eta_1-\eta_2)}$$

η	n=1	n=2	n=3	n=4	n=5	n=6	$\sum_{n=1}^{6}$	Rt.Side (1)	Δ (2)
0°									
1.22	-.875	0.280	-.089	0.027	-.008	0.002	-.663	0.372	0.051
1.26	-.866	0.270	-.082	0.024	-.007	0.002	-.659	0.374	0.029
1.30	-.858	0.261	-.077	0.022	-.006	0.002	-.656	0.376	0.008
1.34	-.853	0.254	-.072	0.020	-.005	0.001	-.655	0.376	-.010
40°									
1.22	-.558	-.062	0.092	-.033	0.003	0.005	-.553	0.431	0.062
1.26	-.552	-.060	0.084	-.029	0.003	0.004	-.550	0.433	0.034
1.30	-.548	-.058	0.079	-.026	0.002	0.003	-.548	0.434	0.009
1.34	-.545	-.056	0.074	-.023	0.002	0.003	-.545	0.436	-.016
80°									
1.22	0.138	-.283	-.095	0.009	0.012	-.003	-.222	0.610	0.161
1.26	0.137	-.273	-.087	0.008	0.010	-.003	-.208	0.617	0.100
1.30	0.136	-.264	-.082	0.007	0.009	-.002	-.196	0.624	0.042
1.34	0.135	-.257	-.077	0.006	0.007	-.002	-.188	0.628	-.010
120°									
1.22	0.628	0.000	-.073	0.036	0.009	0.000	0.600	1.054	0.204
1.26	0.621	0.000	-.067	0.032	0.007	0.000	0.593	1.050	0.083
1.30	0.618	0.000	-.063	0.028	0.006	0.000	0.589	1.048	-.027
1.34	0.612	0.000	-.059	0.026	0.005	0.000	0.584	1.045	-.124
180°									
1.22	0.885	0.295	0.101	0.034	0.012	0.004	1.331	1.448	0.400
1.26	0.876	0.284	0.093	0.030	0.010	0.004	1.297	1.430	0.181
1.30	0.868	0.275	0.087	0.027	0.008	0.003	1.268	1.414	-.007
1.34	0.863	0.267	0.082	0.025	0.007	0.002	1.264	1.403	-.161
200°									
1.22	0.877	0.253	0.092	0.029	0.009	0.003	1.263	1.412	0.409
1.26	0.868	0.243	0.084	0.026	0.007	0.002	1.230	1.394	0.197
1.30	0.860	0.236	0.079	0.023	0.006	0.002	1.206	1.381	0.010
1.34	0.856	0.229	0.074	0.021	0.005	0.002	1.187	1.371	-.150
240°									
1.22	0.718	0.226	-.032	-.029	-.012	-.004	0.867	1.198	0.222
1.26	0.711	0.217	-.029	-.026	-.010	-.003	0.860	1.194	0.074
1.30	0.705	0.210	-.027	-.023	-.009	-.003	0.853	1.190	-.059
1.34	0.700	0.204	-.026	-.021	-.007	-.002	0.848	1.188	-.177

(1) $\text{Rt. Side} = \frac{d}{a}\left[\frac{1}{\eta_1-\eta_2} + 2\sum_{n=1}^{\infty}(-1)^n e^{-n\eta_2}\cdot\frac{n\cosh n(\eta_1-\eta)\cos n\xi}{\sinh n(\eta_1-\eta_2)}\right]$

(2) $\Delta = \frac{\cosh\eta_1+\cos\xi\cosh(\eta_1-\eta)}{(\cosh\eta+\cos\xi)^2} - \frac{d}{a}\left[\frac{1}{\eta_1-\eta_2}+2\sum_{n=1}^{\infty}(-1)^n n\cdot e^{-n\eta_2}\frac{\cosh n(\eta_1-\eta)\cos n\xi}{\sinh n(\eta_1-\eta_2)}\right]$

GRAPHICAL DETERMINATION OF η MAX

ERROR VS. η

$$\text{ERROR} = -\left[\frac{\cosh\eta_1 + \cos\xi\cosh(\eta_1-\eta)}{(\cosh\eta+\cos\xi)^2}\right] + \frac{d}{a}\left[\frac{1}{\eta_1-\eta_2} + 2\sum_{n=1}^{\infty}(-1)^n n e^{-n\eta}\frac{\cosh n(\eta_1-\eta)\cos n\xi}{\sinh n(\eta_1-\eta_2)}\right]$$

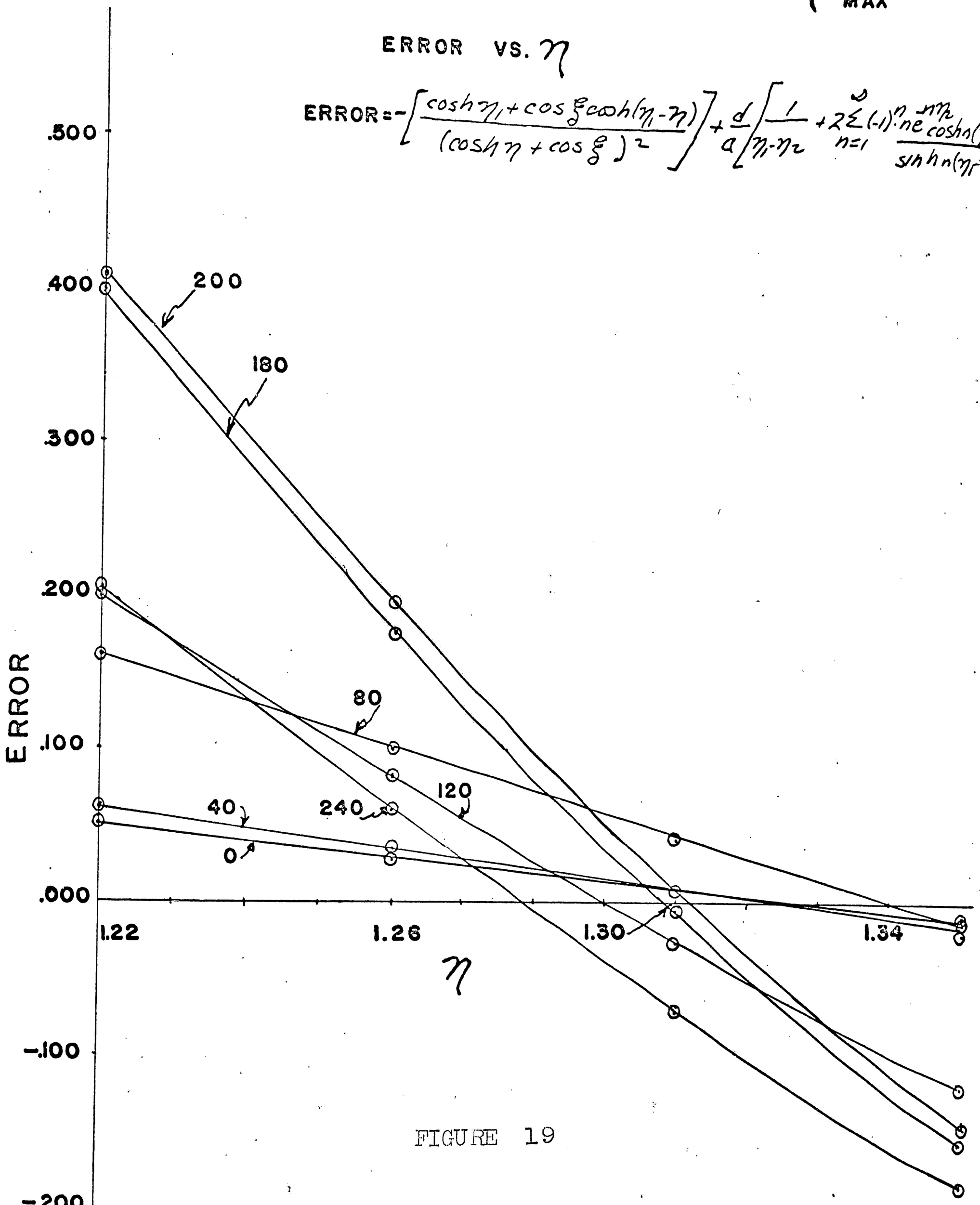

FIGURE 19

From Figure 19 the following values of η_{MAX} are obtained:

Traverse angle	η max
0°	1.32
40°	1.31
80°	1.34
120°	1.29
180°	1.30
200°	1.30
240°	1.28

Calculation of η_{max} by the approximate method of Noyes- R.N. Noyes observed that the points on the line of maximum velocity approximately bisect the circular arcs, which are normal to circles A and B, of the family ξ = constant. From this Noyes developed the following equation for the approximate location of the maxima locus.

$$\eta^* = \operatorname{sech}^{-1}\left\{\sqrt{(1-\tanh\eta_1)(1+\tanh\eta_2)} + \sqrt{(1+\tanh\eta_1)(1-\tanh\eta_2)}\right\}\frac{1}{2}$$

for the system investigated

$$\eta^* = \operatorname{sech}^{-1}\left\{\sqrt{(1-.90515)(1+.81102)} + \sqrt{(1+.90515)(1-.81102)}\right\}\frac{1}{2}$$

$$= \operatorname{sech}^{-1}\frac{1}{2}\{1.0145\} = \underline{1.30}$$

To construct this circle its center must be located and its radius determined.

Radius $a^* = c/\sinh\eta^* = 2.12/1.698 = 1.25$

Center $[c\coth\eta^* 0] = [2.12 \times 1.1605, 0] = [2.460, 0]$

Difference Between Calculated And Measured Maximum Velocity Position - To evaluate the error in terms of percent of traverse distance the $\Delta\eta$ corresponding to a 20% change in position along the traverse was calculated and employed to extrapolate the error associated with the reported differences in η, i.e., η_{exp} $\eta_{Navier\ Stokes}$. Table 7 presents the summary of these calculations.

TABLE 7

Change of η Corresponding To A Distance Change Of 20% Of The Total Traverse Distance

Traverse angle	Position 1			Position 2			$\frac{\Delta\eta}{20\%}$
	V_1	V_2	η_1	V_1	V_2	η	
0	33.21	9.88	1.21	34.04	8.60	1.38	0.17
40	35.51	9.88	1.28	26.30	9.00	1.39	0.11
80	42.80	11.87	1.28	42.79	11.10	1.35	0.07
120	51.32	14.19	1.29	50.88	13.54	1.32	0.03
180	58.73	16.27	1.28	58.32	15.94	1.35	0.07
200	58.30	16.15	1.28	58.10	15.92	1.30	0.02
240	53.35	15.80	1.22	53.00	14.79	1.28	0.06

Note: Measuring from an experimentally determined maximum velocity point along a traverse line all position 1 points are located 10 percent of the traverse distance closer to the shell, while all position 2 points are located 10 percent of the traverse distance closer to the core.

APPENDIX C

Calculation Of Point Velocities From Experimental Data:

All numbers from Run No. 36 Sequence 4

Null Height	6.665"	6.645"
Null Reading	0.6	8.5

Sensitivity of microscope scale .020/7.9 .00254"/unit

Reservoir height for equilibrium at sequence 4-- 6.960"

Scale reading ---------- 5.9

Change in height uncorrected ---------- 0.295"

Correction for scale reading--5.2x.00254-------- 0.013"

Correscted△reservoir height ---------- 0.308"

$$V = C_i \sqrt{2 g_c \frac{\Delta P}{\rho}} \qquad C_i = 1.0$$

$$V = \sqrt{\frac{2 \times 32.2 \frac{\#m}{\#f} \frac{ft}{sec^2} \times 60.5 \#m\,oil \times \Delta Hgt'' \times \frac{1 ft}{12 in} \times \frac{\#f}{\#m}}{.0704 \frac{\#m\,oil}{ft^3}}}$$

$$V = \sqrt{7.162 \times \Delta Hgt'' \times 10^2} = \sqrt{1420.50} = \underline{37.7 fps}$$

TABLE 8

Experimental Point Velocity Data For Turbulent Flow In An Eccentric Annulus

Velocity (ft/sec)	Location of point velocity from outer shell 0 traverse	40 traverse	80 traverse	120 traverse
Maximum pt.	.417	.420	.335	.239
20.0	wall	wall	wall	.030-.406
21.8	wall	wall	wall	.054-.349
26.0	wall	.020-.741	.032-.601	.140-.317
27.6	wall	.038-.740	.058-.586	.239
30.0	.046-.765	.069-.718	.102-.558	
32.0	.074-.747	.092-.695	.147-.524	
35.0	.121-.713	.150-.653	.247-.430	
35.7	.134-.692	.167-.640	.300-.371	
38.0	.181-.663	.220-.592		
40.0	.273-.568	.295-.523		

Velocity (ft/sec)	180 traverse	200 traverse	240 traverse
Maximum pt.	.130	.128	.220
20.0	.078-.174	.107-.152	.035-.360
21.8	.130		
26.0			.130-.294
27.6			.220

Note: All data presented above was determined from the velocity profiles presented in Figures 7 to 12. All distances are stated in inches from outer shell. This data is plotted in Figure 6.

APPENDIX D

EXPERIMENTAL DATA

Run No. 33 Top Position Traverse Distance 0.802"
Traverse Angle 0

Null height	6.671"	6.651"	
Null reading	-0.8	8.8	

Sequence	℄ from OW	Res Hgt	Scale Rdg.	T	ΔHgt.	u(fps)
1	.738	6.822	1.0 ± 1.5	104.6	0.155	26.76
2	.021	6.822	5.5 ± 1.0	105.0	0.164	27.53
3	.121	6.933	3.5 ± 1.0	105.0	0.271	25.38
4	.221	7.007	0.8 ± 1.0	105.7	0.339	29.57
5	.321	7.045	2.7 ± 0.7	105.4	0.381	41.95
6	.421	7.058	4.7 ± 1.0	105.4	0.398	42.87
7	.521	7.042	5.2 ± 0.7	105.4	0.383	42.07
8	.621	7.007	0.5 ± 0.5	105.0	0.339	39.58
9	.721	6.912	5.5 ± 1.0	105.0	0.254	34.26

Run No. 34 Top Position Traverse Distance 0.803"
Traverse Angle 0

Nullheight	6.646	6.667	6.646
Null reading	9.2	0.3	9.0

Sequence	℄ From OW	Res Hgt.	Scale Reading		T	ΔHgt	u(Fps)
1	.021	6.831	3.5	1.5	104.5	0.172	28.19
2	.782	6.831	5.8	1.3	105.3	0.177	28.60
3	.721	6.922	0.9	1.0	105.8	0.256	34.39
4	.621	7.008	-.5	1.0	105.5	0.339	39.57
5	.521	7.046	3.8	1.0	105.0	0.387	42.28
9	.471	7.056	1.5	1.0	105.0	0.392	42.56
6	.421	7.066	1.0	1.0	105.5	0.400	42.99
10	.371	7.056	0.0	1.0	105.0	0.388	42.34
7	.321	7.044	1.0	1.0	105.0	0.377	41.73
8	.221	6.997	0.2	0.9	105.0	0.330	39.05
11	.121	6.926	2.0	1.0	105.0	0.263	34.86

Run No. 35 Top Position

Traverse Distance 0.435"
Traverse Angle 120

Null height	6.663	6.647
Null reading	1.0	8.3

Sequence	℄ from OW	Res. Hgt	Scale Rdg	T	ΔHgt	u(ft/sec)
1	0.021	6.726	7.0 ± 1.0	104.1	0.076	18.74
9	0.071	6.766	5.0 ± 1.0	105.1	0.113	22.85
2	0.121	6.796	5.8 ± 1.0	104.2	0.144	25.79
8	0.161	6.806	4.5 ± 1.0	105.1	0.152	26.50
10	0.191	6.810	7.7 ± 1.0	104.2	0.162	27.36
3	0.221	6.813	7.5 ± 1.5	105.1	0.164	27.53
7	0.251	6.820	4.0 ± 1.0	105.0	0.164	27.53
11	0.281	6.813	4.2 ± 1.0	105.3	0.158	27.01
4	0.321	6.810	4.0 ± 1.0	104.6	0.154	26.68
6	0.371	6.798	6.0 ± 1.0	105.0	0.146	26.01
5	0.414	6.720	6.2 ± 1.0	104.6	0.069	17.84

Run No. 36 Top Position

Traverse Distance 0.761
Traverse Angle 40

Null height	6.665	6.645
Null reading	0.6	8.5

Sequence	℄ from OW	Res. Hgt.	Scale Rdg	T	Δ Hgt.	u(ft/sec)
1	0.740	6.806	8.3 ± 1.0	106.0	0.161	27.27
2	0.021	6.795	5.5 ± 1.0	105.7	0.142	25.61
3	0.121	6.903	6.4 ± 1.0	105.5	0.253	34.18
4	0.221	6.960	5.8 ± 1.0	105.2	0.308	37.71
10	0.271	6.990	5.3 ± 1.0	104.0	0.337	39.45
5	0.321	7.002	7.2 ± 1.0	105.0	0.354	40.45
11	0.371	7.022	2.7 ± 1.0	104.0	0.361	40.85
6	0.421	7.020	5.0 ± 1.0	104.6	0.366	41.12
9	0.471	7.013	6.2 ± 1.0	104.0	0.362	40.90
7	0.521	6.998	6.0 ± 1.0	104.5	0.347	40.04
8	0.621	6.948	5.0 ± 1.0	104.5	0.294	36.86

Run No.38 Top Position Traverse Distance 0.251
Traverse Angle 180

Null height	6.666	6.645
Null reading	0.4	9.0

Sequence	℄from OW	Res.Hgt.	Scale Rdg.	T	ΔHgt.	u(ft/sec)
1	0.230	6.695	2.0 ± 1.0	105.5	0.032	12.16
2	0.021	6.695	5.0 ± 1.0	105.0	0.039	13.45
4	0.111	6.758	4.0 ± 1.0	105.0	0.100	21.45
5	0.121	6.758	4.5 ± 1.0	105.0	0.102	21.71
6	0.141	6.758	4.5 ± 1.0	105.0	0.102	21.71
3	0.161	6.758	2.5 ± 2.0	105.0	0.097	21.17
7	0.191	6.739	3.5 ± 1.0	105.0	0.080	19.23
8	0.179	6.739	6.5 ± 1.0	105.5	0.086	19.93
9	0.051	6.728	4.0 ± 1.0	105.5	0.070	17.99
10	0.210	6.700	4.0 ± 1.0	105.5	0.042	13.93

Run No. 39 Top Position Traverse Distance 0.625
Traverse Angle 80

Null height	6.665	6.649
Null reading	0.3	9.0

Sequence	℄from OW	Res.Hgt.	Scale Rdg.	T	ΔHgt	u(ft/sec)
1	0.605	6.787	7.5 ± 1.0	105.0	0.135	24.97
2	0.021	6.798	5.0 ± 1.0	104.9	0.141	25.52
3	0.121	6.870	4.5 ± 1.0	104.1	0.213	31.37
4	0.221	6.914	6.0 ± 1.0	104.1	0.261	34.66
8	0.271	6.923	7.0 ± 1.0	104.2	0.270	35.32
5	0.321	6.946	2.5 ± 1.0	104.2	0.285	36.28
9	0.371	6.937	3.8 ± 1.0	104.2	0.278	35.84
6	0.421	6.921	6.3 ± 1.0	104.2	0.267	35.12
7	0.521	6.887	4.5 ± 1.0	104.2	0.230	32.60

Run No. 40 Top Position Traverse Distance 0.398
Traverse Angle 240

Null height	6.665	6.647
Null reading	1.3	8.0

Sequence	℄from OW	Res.Hgt	Scale Rdg.	T	ΔHgt	u(ft/sec)
1	0.021	6.724	8.0 ± 1.0	106.0	0.077	18.86
2	0.121	6.803	5.5 ± 1.5	106.5	0.149	26.24
7	0.171	6.811	5.0 ± 1.5	106.0	0.156	26.84
3	0.221	6.828	1.8 ± 1.5	106.5	0.164	27.53
6	0.271	6.801	9.2 ± 1.0	106.0	0.157	26.94
4	0.321	6.782	6.0 ± 1.0	106.3	0.130	24.51
5	0.372	6.712	5.5 ± 1.0	106.0	0.058	16.37

Run No. 41 Top Position

Traverse Distance 0.767
Traverse Angle 40

Null height	6.664	6.445
Null reading	1.2	9.0

Sequence	℄from OW	Res Hgt.	Scale Rdg.	T	ΔHgt.	u(ft/sec)
3	0.412	7.043	0.5 ±2.0	104.2	0.377	41.73
1	0.521	7.016	1.0 ±1.5	104.6	0.351	40.27
2	0.621	6.962	2.5 ±1.0	104.2	0.302	37.35
4	0.121	6.907	4.5 ±1.0	104.5	0.252	34.12

Run No. 42 Top Position

Traverse Diatance 0.632
Traverse Angle 80

Null height	6.666	6.648
Null reading	0.4	8.2

Sequence	℄from OW	Res Hgt.	Scale Rdg.	T	ΔHgt.	u(ft/sec)
1	0.611	6.794	5.5 ±1.0	104.6	0.140	25.43
2	0.497	6.897	4.5 ±1.5	105.0	0.241	33.34
3	0.397	6.943	-.5 ±1.0	105.2	0.275	35.65
4	0.347	6.943	1.5 ±1.0	105.2	0.280	35/96
5	0.297	6.943	0.0 ±1.0	105.5	0.276	35.71
6	0.247	6.907	7.0 ±1.5	105.5	0.257	34.46
7	0.197	6.890	8.5 ±1.0	105.5	0.243	33.51
8	0.097	6.845	4.5 ±1.5	105.5	0.189	29.55
9	0.021	6.795	5.0 ±1.5	105.5	0.139	25.34

Meniscus history taken during sequence 1

Time (sec)	Scale Reading	Time (sec)	Scale Reading
0	4.7	0	5.8
5	5.2	5	5.3
10	3.9	10	4.7
15	6.8	15	5.1
20	4.0	20	6.4
25	4.9	25	4.0
30	3.2	30	4.2
35	4.6	35	3.8
40	5.4	40	5.0
45	7.2	45	5.1
50	5.0	50	4.2
55	6.4	55	4.8
60	6.2	60	5.8

Run No. 43 Top Position

Traverse Distance 0.260
Traverse Angle 200

Null height	6.647	6.664
Null reading	9.0	0.3

Sequence	℄from OW	Res Hgt.	Scale Rdg	T	ΔHgt.	u(ft/sec)
1	.021	6.685	3.5 ± 1.5	105.0	.027	11.17
2	.050	6.718	2.5 ± 1.5	105.1	.058	16.37
3	.100	6.747	1.5 ± 1.5	105.5	.085	19.82
4	.110	6.747	2.5 ± 1.0	105.5	.084	19.71
5	.125	6.747	3.2 ± 1.0	105.8	.089	20.28
10	.125	6.744	4.0 ± 1.0	105.4	.090	20.39
6	.140	6.747	2.5 ± 1.9	105.9	.087	20.04
7	.170	6.747	0.5 ± 1.5	105.5	.083	19.59
8	.200	6.722	4.0 ± 1.9	105.4	.065	17.33
9	.239	6.659	7.5 ± 1.9	105.4	.011	7.13

Run No. 44 Top Position

Traverse Distance 0.258
Traverse Angle 200

Null height	6.662	6.644
Null reading	3.4	9.9

Sequence	℄from OW	Res Hgt	Scale Rdg	T	ΔHgt.	u(ft/sec)
1	.237	6.690	-.5 ± 0.5	107.0	.018	9.12
2	.137	6.759	0.5 ± 1.0	107.5	.088	20.14
3	.167	6.756	0.5 ± 1.0	108.0	.085	19.82
4	.097	6.745	4.2 ± 1.0	108.0	.085	19.82
5	.047	6.703	10.0 ± 0.5	107.0	.059	16.51

Run No. 45 Position 2ft from bottom

Traverse Distance 0.757
Traverse Angle 40

Null height	6.668	6.651
Null reading	0.5	8.0

Sequence	℄from OW	Res Hgt	Scale Rdg	T	ΔHgt	u(ft/sec)
1	.021	6.791	0.5 ± 1.0	103.8	.123	23.84
2	.071	6.870	1.0 ± 1.0	104.5	.203	30.62
3	.171	6.953	2.5 ± 1.0	105.0	.289	36.52
4	.271	7.006	3.5 ± 1.0	105.0	.345	39.94
5	.371	7.034	3.2 ± 1.0	105.3	.372	41.45
6	.471	7.034	0.8 ± 1.0	105.4	.366	41.12
7	.571	6.989	2.5 ± 1.0	105.4	.326	38.82
8	.671	6.917	3.0 ± 1.5	105.4	.255	34.32
9	.701	6.891	4.0 ± 1.5	105.4	.231	32.66

APPENDIX E

Thermocouple Calibration

Thermocouple	Temperature in Dewar, F°	EMF Read	Emf of St'd Copper Constantan Thermocouple
	45.89	1.851	1.845
	40.70	1.626	1.624
	38.31	1.527	1.526
	33.09	1.306	1.308
	45.90	1.853	1.846
	40.70	1.624	1.624
	38.30	1.528	1.526
	33.10	1.306	1.308
	45.84	1.852	1.843
	40.71	1.633	1.625
	38.29	1.526	1.526
	33.10	1.307	1.308

Note: From the agreement between the standard copper constantan and the couples employed it is assumed that the standard thermocouple calibration for copper constantan is applicable.

NOMENCLATURE

Notation Used In Appendix A

A_1	total area between inner cylinder and line of maximum velocities, sq ft
A_2	total area between outer cylinder and line of maximum velocities, sq ft
g_c	conversion factor, 32.2 ft/sec^2
ℓ	peripheral distance along wall, ft
p	static pressure, lb/sq ft abs
r	radius, ft
u	time-averaged velocity parallel to wall at a point, ft/sec
u_b	local bulk velocity at a cross section of annulus ft/sec
u_m	velocity at a point on line of maximum velocities, ft/sec
x	axial distance along annulus, ft
y	normal distance from wall, ft
y_{1m}	value of y_1 at u u_m, ft
y_{2m}	value of y_2 at u u_m, ft
μ	absolute viscosity of fluid, (lb)(sec)/sq ft
ρ	mass density, (lb) (sec^2)/ ft^4
τ	shear stress in fluid, lb/ sq ft
Re	Reynolds number,
u^+	velocity parameter, $u/\sqrt{\tau_0/\rho_0}$
u_1^+	velocity parameter, $u/\sqrt{\tau_1/\rho}$
u_2^+	velocity parameter, $u/\sqrt{\tau_2/\rho}$

u_{1m}^+	u_1^+ evaluated at line of maximum velocities
u_{2m}^+	u_2^+ evaluated at line of maximum velocities
y_1^+	wall-distance parameter $\frac{\sqrt{\tau_1/\rho}}{\nu/\rho} y_1$
y_2^+	wall-distance parameter $\frac{\sqrt{\tau_2/\rho}}{\nu/\rho} y_2$
y_{1m}^+	y_1^+ evaluated at line of maximum velocities
y_{2m}^+	y_2^+ evaluated at line of maximum velocities

subscripts:

1	pertaining to inner circle
2	pertaining to outer circle

Notation Used In Appendix B

A	core ($\eta_1 = \eta$ circle)
a	radius of core
B	shell ($\eta_2 = \eta$ circle)
b	radius of shell
c	distance defined in Figure
d	distance between centers of core and shell
L	axial flow direction
P	static pressure
$s = a/b$	radius parameter
v	point velocity
x	cartesian coordinate } defining complex z plane
y	cartesian coordinate } defining complex z plane
$\varepsilon = d/b-a$	eccentricity parameter
$\zeta = \frac{c+z}{c-z}$	complex variable

η	bipolar coordinate
μ	fluid viscosity
ξ	bipolar coordinate
$w = \xi + i\eta$	complex variable

B I B L I O G R A P H Y

1. " Aerodynamic Measurements", Gas Turbine Laboratory, M.I.T., (1953)

2. Cataneo, F.C., M.S. Thesis, Lehigh University, Bethlehem (1960)

3. Deissler, R.G., and Taylor, M.F.: NACA TN 3451, (1955)

4. Folsom, H.G., Trans. A.S.M.E. 78, 1447 (1957)

5. Heyda, J.F. : General Electric Co. Report, APEX-391, (1958)

6. Hinze, J.O., "Turbulence", M^{c}-Graw-Hill Book Company, Inc., New York (1959)

7. Knudsen, J.G. and Katz, D.L., Proc. Midwestern Conf. on Fluid Dynamics, 1st Conf., No.2, 175 (1950)

8. Pankhurst, R.C., and Holder, D.W., "Wind-Tunnel Technique", Sir Issac Pitman & Sons Ltd., London (1948)

9. Redberger, P.J., and Charles, M.E., Can. J. Chem. Eng., 40: No.4, 148 (1962)

10. Rothfus, R.R., Ph.D. Thesis, Carnagie Institute of Technology (1948)

11. Rothfus, R.R., Monrad, C.C., and Senecal, V.E., Ind. Eng. Chem., 42, 2511 (1950)

12. Rothfus, R.R., Monrad, C.C., Sikchi, K.G. and Heideger, W.J., Ind. Eng. Chem., 47, No.5, 913 (1955)

13. von Karman, Th., : Jour. Aero. Sci., vol.1, no.1, 1 (1934)

14. Walker, J.E., Whan, G.A., and Rothfus, R.R., A.I.Ch.E. Journal 3, No.4, 485 (1957)

VITA

The author was born on March 15, 1938 in Washington, D.C., the son of Samuel and Alice Wolffe.

Upon graduation from Woodrow Wilson High School in Washington he attended the University of Maryland in College Park, Maryland, and received a B.S. in Ch.E. and The Merck Award in Chemistry and Chemical Engineering from that institution in June 1960.

In the fall of 1960 he enrolled in the Graduate School of Lehigh University and assumed the responsibilities of a graduate teaching assistant in Chemical Engineering. The position of graduate assistant was retained until the fall of 1962 when he received a California Oil Fellowship in Chemical Engineering.

The author is a member of Alpha Chi Sigma (chemical professional fraternity) and the A.I.Ch.E.